Differential roles of α-, β-, and γ-actin in axon growth and collateral branch formation in motoneurons

Mehri Moradi,[1] Rajeeve Sivadasan,[1] Lena Saal,[1] Patrick Lüningschrör,[1] Benjamin Dombert,[1] Reena Jagdish Rathod,[1] Daniela C. Dieterich,[2,3] Robert Blum,[1] and Michael Sendtner[1]

[1]Institute of Clinical Neurobiology, University Hospital Wuerzburg, University of Wuerzburg, 97078 Wuerzburg, Germany
[2]Institute for Pharmacology and Toxicology and [3]Center for Behavioral Brain Sciences, Medical Faculty, University of Magdeburg, 39120 Magdeburg, Germany

Axonal branching and terminal arborization are fundamental events during the establishment of synaptic connectivity. They are triggered by assembly of actin filaments along axon shafts giving rise to filopodia. The specific contribution of the three actin isoforms, Actα, Actβ, and Actγ, to filopodia stability and dynamics during this process is not well understood. Here, we report that Actα, Actβ, and Actγ isoforms are expressed in primary mouse motoneurons and their transcripts are translocated into axons. shRNA-mediated depletion of Actα reduces axonal filopodia dynamics and disturbs collateral branch formation. Knockdown of Actβ reduces dynamic movements of growth cone filopodia and impairs presynaptic differentiation. Ablation of Actβ or Actγ leads to compensatory up-regulation of the two other isoforms, which allows maintenance of total actin levels and preserves F-actin polymerization. Collectively, our data provide evidence for specific roles of different actin isoforms in spatial regulation of actin dynamics and stability in axons of developing motoneurons.

Introduction

Cytoskeletal dynamics plays a pivotal role in the establishment of neuronal connections during development and in plasticity in adults. Actin turnover is particularly crucial for axon elongation, guidance, arborization, and synapse assembly (Campbell and Holt, 2001; Zhang and Benson, 2001; Luo, 2002). Actin dynamics appears particularly important for axon arborization in motoneurons, as motor axons establish several thousand branches, each innervating a neuromuscular endplate (Hirokawa et al., 1989). Axonal sprouting as a specific form of arborization plays a major role in the plasticity of motor units (Tam and Gordon, 2003; Gordon and Tyreman, 2010). In the early stages of motoneuron disease, sprouting can compensate for loss of motoneurons and delay disease onset, as shown in a model of type III spinal muscular atrophy (SMA; Crawford and Pardo, 1996; Simon et al., 2010). In addition, recent studies in *Caenorhabditis elegans* neuronal development have shown that actin reorganization at presynaptic sites allows simultaneous axonal branching and synapse formation, thus providing a mechanism for synapse-directed sprouting (Chia et al., 2014).

Axonal branching initiates with polymerization of F-actin at branch sites, which leads to filopodia formation. Subsequent microtubule invasion and polymerization are then required for maturation of nascent filopodia into branches (Dent and Kalil, 2001; Gallo, 2011; Kalil and Dent, 2014). The dynamics of F-actin polymerization is orchestrated by action of three actin isoforms, Actα, Actβ and Actγ, and several actin-binding proteins (Dwivedy et al., 2007; Bergeron et al., 2010). The role of Actβ in this context has been extensively studied in different neuronal subtypes. In sensory neurons, siRNA depletion of Actβ leads to reduced axon branching (Donnelly et al., 2013). In *Xenopus* retinal ganglion neurons, axonally synthesized Actβ mediates growth cone turning in response to guidance cues (Leung et al., 2006). In mature neurons, Actβ contributes to synaptic plasticity and is synthesized in response to nerve injury during axon regeneration (Micheva et al., 1998; Zheng et al., 2001). In contrast, little is known about the contribution of the other two isoforms, Actα and Actγ. Three actin isoforms are highly similar in their protein sequences and differ only in few amino acids at their N-terminal end, and the corresponding mRNAs show about 90% sequence identity within their coding regions (Vandekerckhove and Weber, 1978). However, the mRNAs for Actα, Actβ, and Actγ differ in their 3′ UTR regions, suggesting that subcellular transport and translation depending on these 3′ UTR regions are differentially regulated. These differences in localization of isoactin transcripts and proteins as well as studies of actin isoform–specific knockout mouse models imply that these isoforms can accomplish specific cellular functions (Perrin and Ervasti, 2010).

Correspondence to Michael Sendtner: sendtner_m@ukw.de

R.J. Rathod's present address is Institute for Stem Cell Biology and Regenerative Medicine, Gandhi Krishi Vigyan Kendra, Bangalore 560065, India.

Abbreviations used: ALS, amyotrophic lateral sclerosis; BDNF, brain-derived neurotrophic factor; CNTF, ciliary neurotrophic factor; DBP, vitamin D–binding protein; DIG, digoxigenin; DIV, days in vitro; E, embryonic day; LNA, locked nucleic acid; PLP, paraformaldehyde lysine phosphate; SMA, spinal muscular atrophy.

The Rockefeller University Press $30.00
J. Cell Biol. Vol. 216 No. 3 793–814
https://doi.org/10.1083/jcb.201604117

We have investigated the contribution of Actα, Actβ, and Actγ to differential regulation of axonal branching and growth cone dynamics in embryonic mouse motoneurons. Using high-resolution in situ hybridization, we show that Actα, Actβ, and Actγ isoforms are endogenously expressed in motoneurons and all three actin isoform–specific mRNAs localize into axons. Interestingly, we found that depletion of Actα associates with disturbed filopodia dynamics and prevents formation of axonal collateral branches, whereas depletion of Actβ reduces dynamics of axonal growth cones and impairs maturation of presynapses. Depletion of Actγ diminishes filopodia dynamics along axons and impairs axonal elongation. Interestingly, depletion of Actα or Actγ caused a shift of Actβ from the F-actin to the G-actin pool, indicating that the stability of Actβ-containing filaments is determined by these two isoforms.

Importantly, our data also reveal that loss of Actβ leads to increased expression of Actα and Actγ. In line with this, we observed that the compensatory up-regulation of Actα and Actγ is sufficient to maintain the total actin levels and F-actin polymerization capacity in the soma. Collectively, these data point to specific functions of Actα, Actβ, and Actγ in axon elongation and plasticity and emphasize a specific role of Actα and Actγ in axonal branching in developing motoneurons.

Results

Actα, Actβ, and Actγ isoforms are expressed in mouse motoneurons, and their mRNAs are targeted to axons

Based on studies that Actβ and Actγ isoforms are present in all neuronal subtypes (Rubenstein, 1990) and that the mRNA for Actα is detectable in hippocampal neurons (Cajigas et al., 2012), we studied the expression of all three actin isoforms in motoneurons from embryonic day 18 (E18) and adult mouse spinal cord using laser capture microdissection followed by quantitative RT-PCR analysis (Fig. 1 A). Transcripts for all three isoforms were detected in microdissected motoneurons from both E18 and adult mice. Absolute quantification revealed that Actα is expressed at relatively low levels compared with Actβ, whereas the levels of Actγ mRNAs are high but still lower than those of Actβ (Fig. 1, B and C). When compared with Gapdh, the expression of all three actin isoforms is high during embryonic stages and decreases in the adult. The identity of microdissected motoneurons was confirmed by quantitative RT-PCR analysis of the motoneuron specific marker ChAT. ChAT was detected in E18 and adult microdissected motoneurons, but not in cultured cerebellar neurons and heart (Fig. 1 D). Previous studies have shown that actin isoforms are differentially distributed within muscle cells, with Actα mRNA being present predominantly in the perinuclear compartment and Actβ mRNA in lamellae at the cell periphery (Taneja and Singer, 1990), and that only Actβ, but not Actγ, mRNA is transported into axons of cortical and sensory neurons (Bassell et al., 1998; Zhang et al., 2001; Willis et al., 2007). Because the zipcode domain in the 3′ UTR of the Actβ mRNA was found to be necessary for axonal transport of this specific mRNA (Kislauskis et al., 1993), it was concluded that Actβ is the predominant isoform of actin that can be locally synthesized in the axonal compartment. The transport mechanism for Actβ appears specific and competes with other mRNAs (e.g., the transcript for GAP-43), indicating that the capacity for axonal translocation of specific mRNAs is limited and highly regulated (Donnelly et al., 2011). We reinvestigated the mRNA levels of Actα, Actβ, and Actγ in axons of motoneurons that had been grown in compartmentalized cultures using microfluidic chambers (Saal et al., 2014; Fig. 1 E). After isolation of total RNA from the axonal compartment, we applied quantitative RT-PCR to quantify the mRNA levels of the different actin isoforms and found that all isoforms are present in the somatodendritic compartment as well as in axons (Fig. 1, F–H). As expected, 18s rRNA and Gapdh mRNA were detectable in RNA samples both from somatodendritic and axonal compartments, whereas Histone H1f0 was not detectable in axonal RNA fractions. Absolute quantification revealed that in the axonal compartment, levels of Actβ mRNA were approximately twofold and fourfold higher than the levels of Actα and Actγ mRNAs, respectively ($P < 0.018$; Fig. 1 H). However, we observed a high enrichment of Actα mRNA in the axonal versus somatodendritic compartment, suggesting that this actin isoform might have an axon-specific regulatory function in motoneurons ($P < 0.0003$; Fig. 1 I).

To confirm the subcellular localization of the different actin mRNAs, we used a high-resolution in situ hybridization (FISH) technique (Taylor et al., 2010). Similarly, we found low levels of Actα in the somatodendritic compartment but relatively high levels in axons (Fig. 2 A). Because the coding regions of different actin mRNAs are highly identical, we used probes mostly mapping to the divergent 3′ UTR regions of these transcripts. Actβ and Actγ transcripts showed abundant expression in the soma and were present in proximal axons and growth cones (Fig. 2, B and C). The relative signal intensity for Actα was lower than for Actβ and Actγ because the 3′ UTR regions of Actβ and Actγ are much longer (700 and 682 bp, respectively) than that of Actα (242 bp), so that the corresponding probes could only cover this short domain (Fig. 2, D–F). To exclude crosshybridization between probes, we performed a triplex assay by simultaneous incubation of cells with all three isoform-specific probes, each having a different fluorescent tag. As shown in Fig. 2 G, we did not detect any overlapping fluorescence signals, confirming the specificity of probes. Moreover, the different localization pattern for Actα, Actβ, and Actγ mRNAs indicates that these transcripts are present in different transport granules. In control assays, probes for both Gapdh mRNA and 18srRNA gave rise to discrete signals in motoneuron axons, whereas no signals were detected using scrambled probes or in "no-probe" assays (Fig. S1, A–D). To further verify the specificity of probes, we performed shRNA-mediated knockdown of individual actin isoforms by using a lentiviral transduction based approach. Compared with control motoneurons, signal intensities of Actα, Actβ, and Actγ transcripts were significantly reduced after repression of the corresponding mRNAs, thus confirming the specificity of the used isoform-specific probes (Fig. S1, E–G). Furthermore, we confirmed the axonal localization of Actα with a different in situ hybridization technique using a locked nucleic acid (LNA) probe (Fig. S1, H and I). Next, we examined the protein levels and localization of actin isoforms using isoform-specific antibodies. In Western blot experiments, we detected all three isoforms in lysates of cultured motoneurons (Fig. 3, A–C). We validated the specificity of the respective antibodies using lysates of actin isoform–specific knockdown motoneuron cultures and observed 60% reduction in Actα ($P < 0.004$), 95% reduction in Actβ ($P < 0.002$), and 85% reduction in Actγ protein levels ($P < 0.005$; Fig. 3 D). Furthermore, immunocytochemical analysis

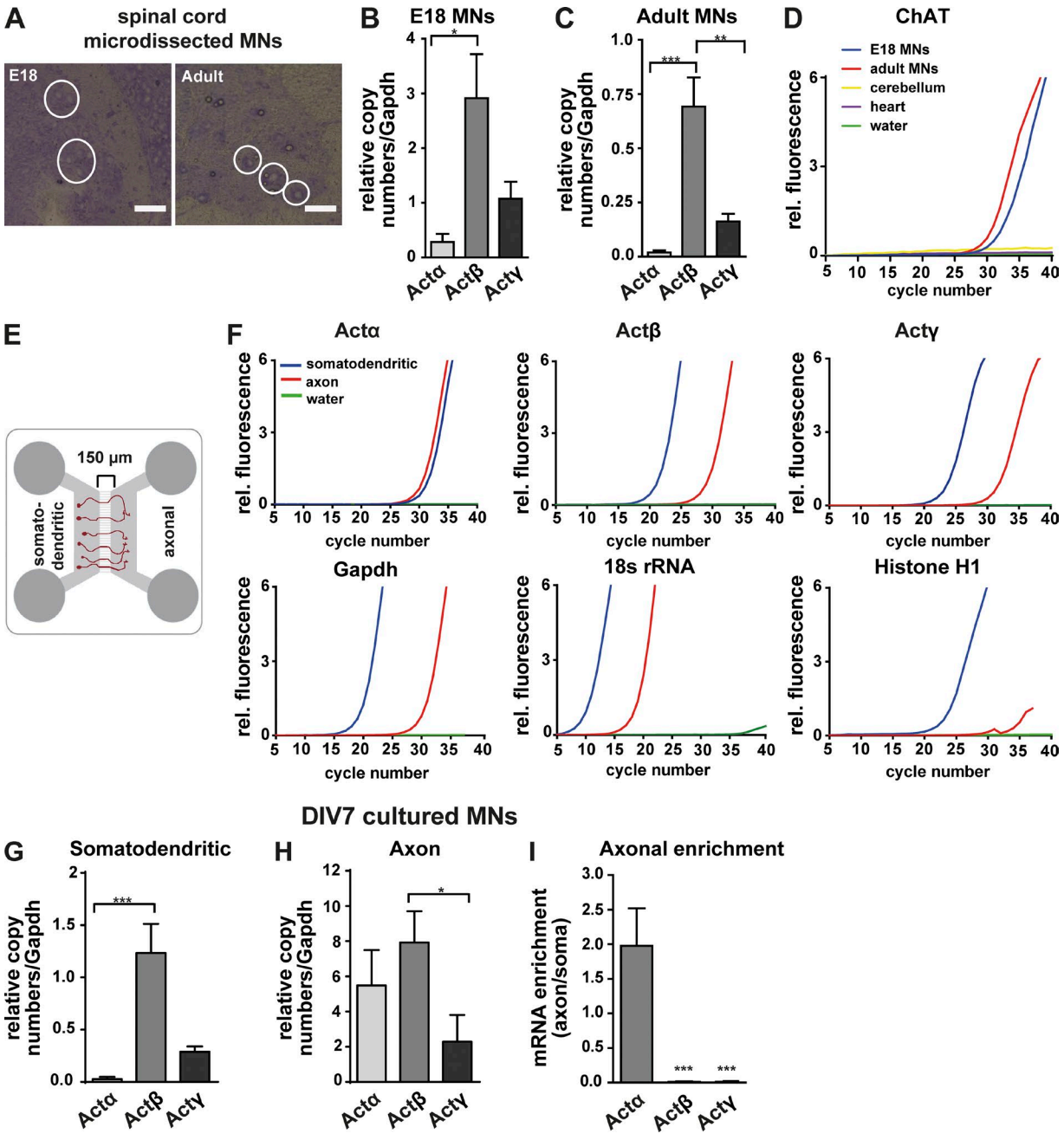

Figure 1. **Actα, Actβ, and Actγ transcripts are found in motoneurons in vivo and in vitro.** (A) Cresyl violet staining of spinal cord sections. Somata of motoneurons (MNs; white circles) were cut from ventral horn of E18 embryos and adult mice using laser capture microdissection. Bars, 200 µm. RNA was extracted and analyzed by quantitative RT-PCR. (B and C) Absolute copy numbers of mRNAs of actin isoforms were normalized to absolute copies of Gapdh. Actα, Actβ, and Actγ mRNAs are detected in E18 stage ($n = 3$) and adult ($n = 4$) motoneurons (*, $P < 0.05$; **, $P < 0.0016$; ***, $P < 0.0005$). (D) ChAT transcripts were detected in RNA samples of E18 and adult microdissected motoneurons but were undetectable in cultured cerebellar neurons and heart tissues. (E) Motoneuron cultures in microfluidic chambers. Axonal growth toward the axonal compartment was supported by a BDNF gradient. RNA was separately extracted from somatodendritic and axonal compartments and used for quantitative RT-PCR analysis. (F) Quantitative RT-PCR amplification curves for Actα, Actβ, Actγ, Gapdh mRNAs, and 18sRNA obtained from somatodendritic and axonal compartments. Histone H10 mRNAs were detected only in somatodendritic compartments. (G and H) Absolute quantification of quantitative RT-PCR data shows that the mRNA levels of Actβ are higher than mRNA levels of Actα and Actγ in both somatodendritic (***, $P < 0.0004$) and axonal compartments (*, $P < 0.018$ for $n = 6$). (I) Ratio of mRNA levels of actin isoforms in somatodendritic versus axonal compartment revealed a relatively high enrichment of Actα transcripts in the axonal compartment (***, $P < 0.0003$). Shown are mean ± SEM. One-way ANOVA with Bonferroni post hoc test was used for statistical analysis.

of cultured motoneurons revealed that the signal obtained with these antibodies was markedly reduced after corresponding shRNA-mediated knockdown (Fig. S2, C–E). The specificity of Actα antibody was further validated by Western blot analysis of HEK^{293T} cells transfected with HA-Actα, HA-Actβ, or HA-Actγ expression vectors and immunolabeling of motoneurons using HA antibody (Fig. S2, A and B).

Actα immunostaining assay showed that this isoform is present at low levels in the soma or in axonal growth cone filopodia, but it accumulates at axonal branch points (Fig. 3 E). In

contrast to Actα, Actβ and Actγ are abundant in the soma and localize to highly dynamic compartments, in particular to axonal filopodia and axonal growth cone filopodia (Fig. 3, F and G).

This differential subcellular localization of Actα, Actβ, and Actγ appears indicative of specific cellular functions of these isoforms. We therefore asked whether these actin isoforms contribute differentially to F-actin polymerization in different subcellular compartments. We performed live-cell extraction to remove soluble G-actin from motoneurons and stained them with phalloidin and actin isoform–specific antibodies. As shown in Fig. 3 H, filamentous Actα colocalized with phalloidin mostly in the axon and axonal branch points but only poorly in the soma or in the axonal growth cone. Actβ showed high colocalization with phalloidin, particularly in the growth cone and growth cone filopodia, indicating that this isoform incorporates into F-actin in highly dynamic regions (Fig. 3 I). Actγ showed colocalization with F-actin mostly in the soma and in axons (Fig. 3 J). The removal of G-actin was confirmed by immunostaining using vitamin D–binding protein (DBP), which specifically labels G-actin pools (Lee et al., 2013; Fig. S2 F). In addition, we assayed the removal of the globular protein Gapdh and observed a remarkable reduction of corresponding signal (Fig. S2 G).

Actα, Actβ, and Actγ reporters are locally translated in axonal growth cones and within axons at branch points

Next, we performed FRAP experiments to investigate local translation of the different actin isoforms at axonal branch points and in axonal growth cones. We generated individual eGFP^{myr} lentiviral reporter constructs with the respective 3′ UTRs of Actα, Actβ, and Actγ mRNAs (Fig. 4 A). Motoneurons transduced with these constructs expressed eGFP^{myr} throughout axons after 5 d in culture. Distal axons were bleached and eGFP^{myr} fluorescence recovery was monitored for 1 h after bleach (Fig. 4, B and F). Quantification of eGFP^{myr} FRAP in defined regions of interest within growth cones revealed a recovery of ∼60% for all three actin 3′ UTR reporters indicating that mRNAs of all three different actin isoforms are translated in axonal growth cones (Fig. 4, C–E). These data also show that the distinct isoform-specific 3′ UTRs are sufficient for their axonal translocation. To exclude that the observed recovery of eGFP^{myr} signal is caused by diffusion of proteins from the soma and proximal axon or refolding of bleached GFP, we pretreated cells with cycloheximide and anisomycin. As shown in Fig. 4 (C–E), eGFP^{myr} recovery was significantly reduced after treatment with translation blockers ($P < 0.001$), confirming that the eGFP^{myr} reporters are locally translated.

In addition, we observed that reporters for all three actin isoforms are also translated in translation hot spots within the axonal branch points (Fig. 4, F–H). Notably, the recovery rate of the Actα reporter was significantly higher than the recovery rate of Actβ ($P < 0.01$; Fig. 4 G) and Actγ ($P < 0.05$; Fig. 4 H) during the first 20 min after bleach suggesting that intra-axonal synthesis of Actα in branch points might be involved in axon arborization and sprouting.

Depletion of Actα disturbs formation of axonal collateral branches

Enrichment of Actα protein in the axonal branch points and its high rate of local translation in this region prompted us to assess the possible function of this isoform in axonal arborization. For this purpose, we knocked down each of the three actin isoforms in primary motoneurons by lentiviral shRNA transduction. The efficiency of the knockdown lentiviruses was verified by quantitative RT-PCR (Fig. S3, A–C) and Western blot experiments (Fig. 3, A–D). Next, we analyzed the number of collateral branches at 7 d in vitro (DIV7). Only neurites with a minimum length of 40 µm and positively stained for Tau or Tubulin were considered as mature branches (Fig. 5 A). We found that depletion of Actα impairs formation of axonal branches (Fig. 5 B), as the proportion of axons without collateral branches increased ($P < 0.01$) and the number of axons with three or more branches decreased ($P < 0.01$). Unlike Actα, depletion of Actβ increased the number of axonal branches ($P < 0.01$), and depletion of Actγ had no effects on branch formation (Fig. 5, C and D). These results indicate that Actα plays an essential role in formation of axonal collateral branches in motoneurons.

To rule out the possibility that Actα affects cell survival and leads to selection of a subgroup of motoneurons with fewer branches, we assessed the effects of depletion of each actin isoform on cell viability, axon elongation, dendrite length, and dendrite number (Fig. 5 E). We found that depletion of none of the actin isoforms alone affected cell survival (Fig. 5, F–H). Also dendrite length and number were not reduced (Fig. 5, I and J). Intriguingly, we observed a significant reduction of ∼20% in the soma size in Actα-depleted neurons ($P < 0.0001$; Fig. 5 K). Also, axon length was reduced by 29% after Actα depletion ($P < 0.0001$), by 41% after Actβ depletion ($P < 0.0001$), and by 19% after Actγ deletion ($P < 0.0001$; Fig. 5, L–N). To exclude the possibility of off-target effects, we designed multiple individual shRNAs for targeting Actα (Fig. S3 A), Actβ (Fig. S3 B), and Actγ (Fig. S3 C) and analyzed axon length, branching, and growth cone size in motoneurons expressing these constructs. shActα-2 transduction impaired axonal growth ($P < 0.0001$; Fig. S3 D) and collateral branch formation ($P < 0.01$ and $P < 0.05$; Fig. S3 E). shActβ-2 transduction affected axon elongation ($P < 0.0001$; Fig. S3 F) and growth cone maturation ($P < 0.0001$; Fig. S3 G). Expression of both shActγ-2 and shActγ-3 affected axon elongation ($P < 0.012$ and $P < 0.004$; Fig. S3 H) confirming the target specificity of the applied shRNAs. In addition, we performed rescue experiments for Actβ by expressing a shRNA-resistant lentiviral construct of Actβ in motoneurons (Fig. S4 A). Expression of this rescue construct restored Actβ protein levels to 75% ($P < 0.016$; Fig. S4, B–D) and rescued the observed defects in axonal growth ($P < 0.0002$; Fig. S4, E and F) and growth cone maturation ($P < 0.005$ and $P < 0.0003$; Fig. S4, G–I).

Actα and Actγ modulate axonal filopodia dynamics, whereas Actβ regulates growth cone movement and differentiation

Generation of axonal collateral branches requires the formation of filopodia from the axon shaft (Spillane et al., 2011). Extension and dynamics of these filopodia depend on actin filaments. After microtubule invasion, few filopodia mature into branches, whereas the majority retract into the axon (Gallo, 2011). To understand the role of different actin isoforms in this process, we performed live-cell imaging experiments and analyzed the dynamics of axonal filopodia. We transduced primary motoneurons with lentiviral particles that knockdown actin isoforms and coexpress GFP. This allowed us to monitor the dynamics of filopodia movement for 40 min using a GFP illuminator (Fig. 6, A and B). We analyzed dynamics of filopodia by examining four parameters: (1) frequency of filopodia initiation,

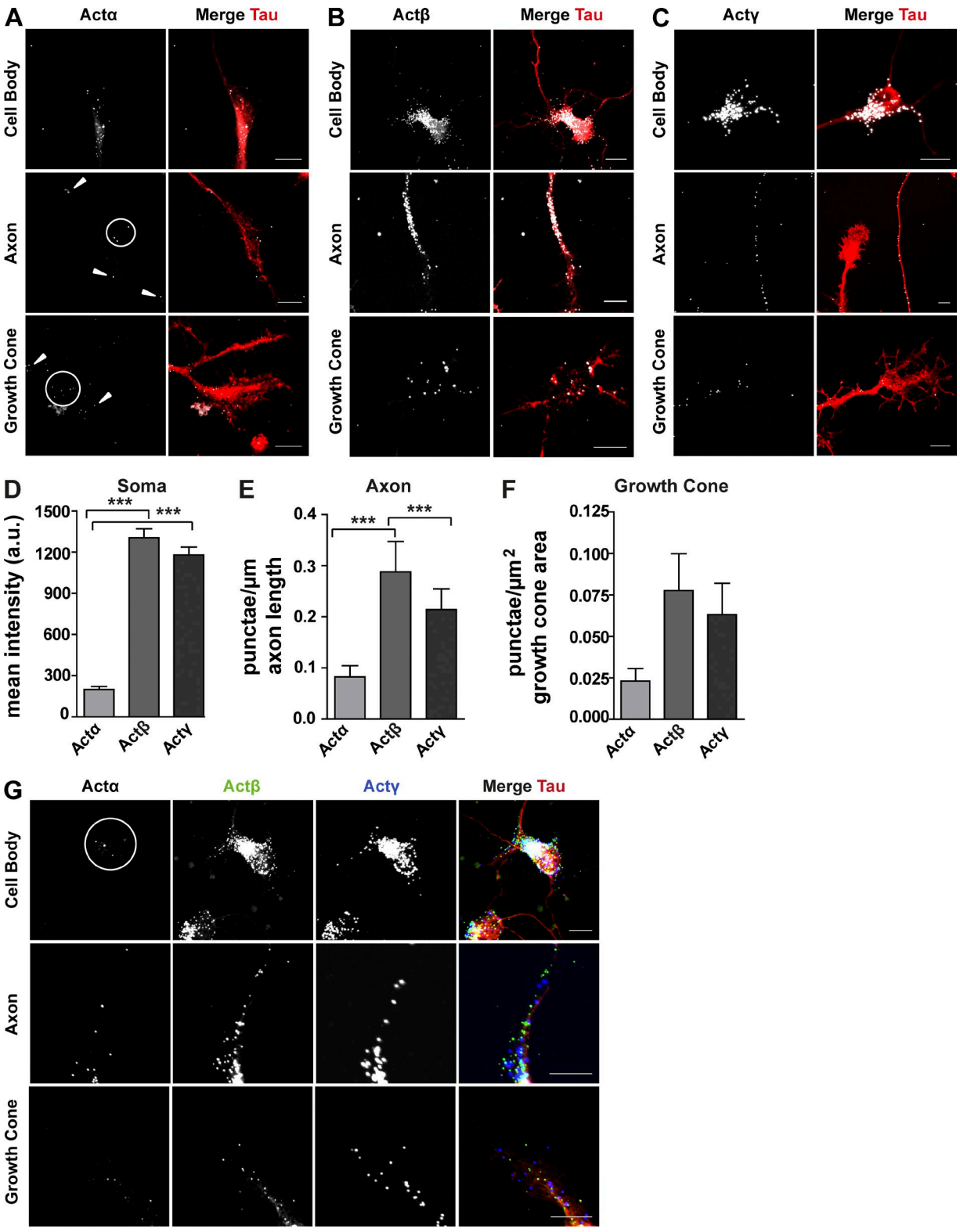

Figure 2. **Subcellular localization of endogenous Actα, Actβ, and Actγ mRNAs in cultured motoneurons.** (A) In situ hybridization signals for Actα (A), Actβ (B), and Actγ transcripts (C) were detected in soma, axons, and axonal growth cones of cultured motoneurons. Cells were immunostained against Tau to determine cell boundaries. (D–F) Quantification of FISH signals shows that Actβ and Actγ are detectable at similar levels in the soma, but Actβ is more abundant in the axon and axonal growth cone (***, $P < 0.0001$ by one-way ANOVA with Dunn's post-test for $n = 6$). Shown are mean ± SEM. (G) In triplex assays, cells were incubated simultaneously with probes detecting transcripts of Actα (white), Actβ (green), and Actγ (blue). Differential localization of actin mRNAs in soma, axons, and growth cones indicates that these mRNAs are present in different RNP granules. White circles and arrowheads in A and G indicate Actα mRNA punctae. Bars, 10 µm.

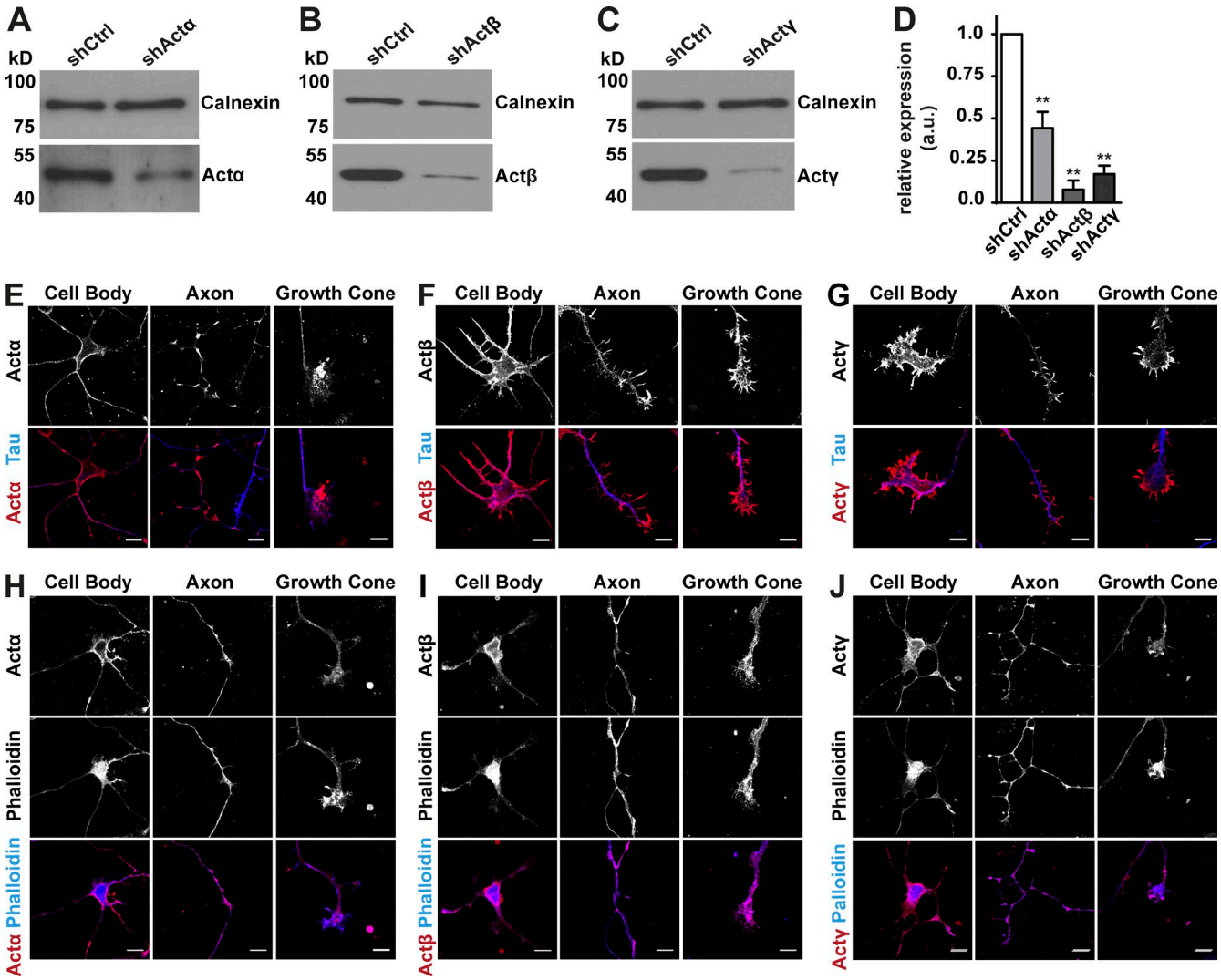

Figure 3. **Actα protein localizes to axonal branch points, whereas Actβ and Actγ are highly enriched in axonal filopodia and axonal growth cones.** (A–C) Immunoblots of total lysates obtained from actin isoform–specific knockdown and control motoneurons probed with specific Actα (A), Actβ (B), and Actγ (C) antibodies. Calnexin was used as loading control. All three isoforms are detected in cultured motoneurons. (D) shRNA-mediated knockdown leads to a 60% reduction in Actα (**, $P < 0.004$ for $n = 4$), a 95% reduction in Actβ (**, $P < 0.002$ for $n = 10$), and a 85% reduction in Actγ (**, $P < 0.005$ for $n = 5$) protein levels (one-tailed Mann-Whitney test). Shown are mean ± SEM. (E–G) Motoneurons were stained against Tau and Actα (E), Actβ (F), and Actγ (G). Actα protein is highly enriched in axonal branch points and neurites (E). Actβ (F) and Actγ proteins (G) are very abundant in the soma and localize to axonal filopodia and axonal growth cone filopodia. (H–J) Motoneurons were extracted using Triton X-100 to remove G-actin. Cells were fixed and stained with phalloidin and Actα (H), Actβ (I), and Actγ (J) antibodies. (H) Colocalization of Actα with phalloidin shows that this isoform incorporates into F-actin in the axon and particularly in the axonal branch points. (I) Filamentous Actβ is present predominantly in the axonal growth cone filopodia. (J) Actγ colocalizes with phalloidin mostly in the soma and axons. Images are representative of three independent experiments. Bars, 10 µm.

(2) filopodia life time, (3) rate of filopodia dynamic movement (how many times a filopodia grew or retracted during the total imaging period), and (4) the total absolute changes in length for individual filopodia. Notably, many filopodia did not show dynamic changes during imaging (35% in control, 47% in shActα knockdown, 34% in shActβ knockdown, and 57% in shActγ knockdown). Among those showing dynamic movements, we found that knockdown of either Actα or Actγ decreases the filopodia initiation rate by 60% and knockdown of Actβ by 25% (Fig. 6 C). Filopodia lifetime of Actα-depleted neurons was significantly decreased compared with control ($P < 0.010$) and Actβ-depleted neurons ($P < 0.0008$; Fig. 6 D). Also, the rate of filopodia dynamic movements was reduced after knockdown of either Actα or Actγ (Videos 1, 2, and 4). In the control group, individual filopodia underwent on average 14 times dynamic movements during the total imaging period, whereas Actα- and Actγ-depleted filopodia showed a frequency of seven times ($P < 0.0001$; Fig. 6 E). In contrast, the frequency of dynamic movement of Actβ-depleted filopodia was not significantly different from control (Fig. 6 E and Video 3).

We also measured the total change in filopodia length by summing up the absolute changes in filopodia length between consecutive frames. As shown in Fig. 6 F, depletion of either Actα or Actγ caused a 57% reduction ($P < 0.0001$) in the total change in filopodia length (10 and 11 µm, respectively). Again, Actβ-depleted filopodia were similar to controls (17 µm compared with 23 µm in control group; Fig. 6 F). Furthermore, we analyzed axonal filopodia in fixed phalloidin-labeled neurons and found that suppression of Actα affects formation of axonal filopodia ($P < 0.043$; Fig. 6 G). Together, these data

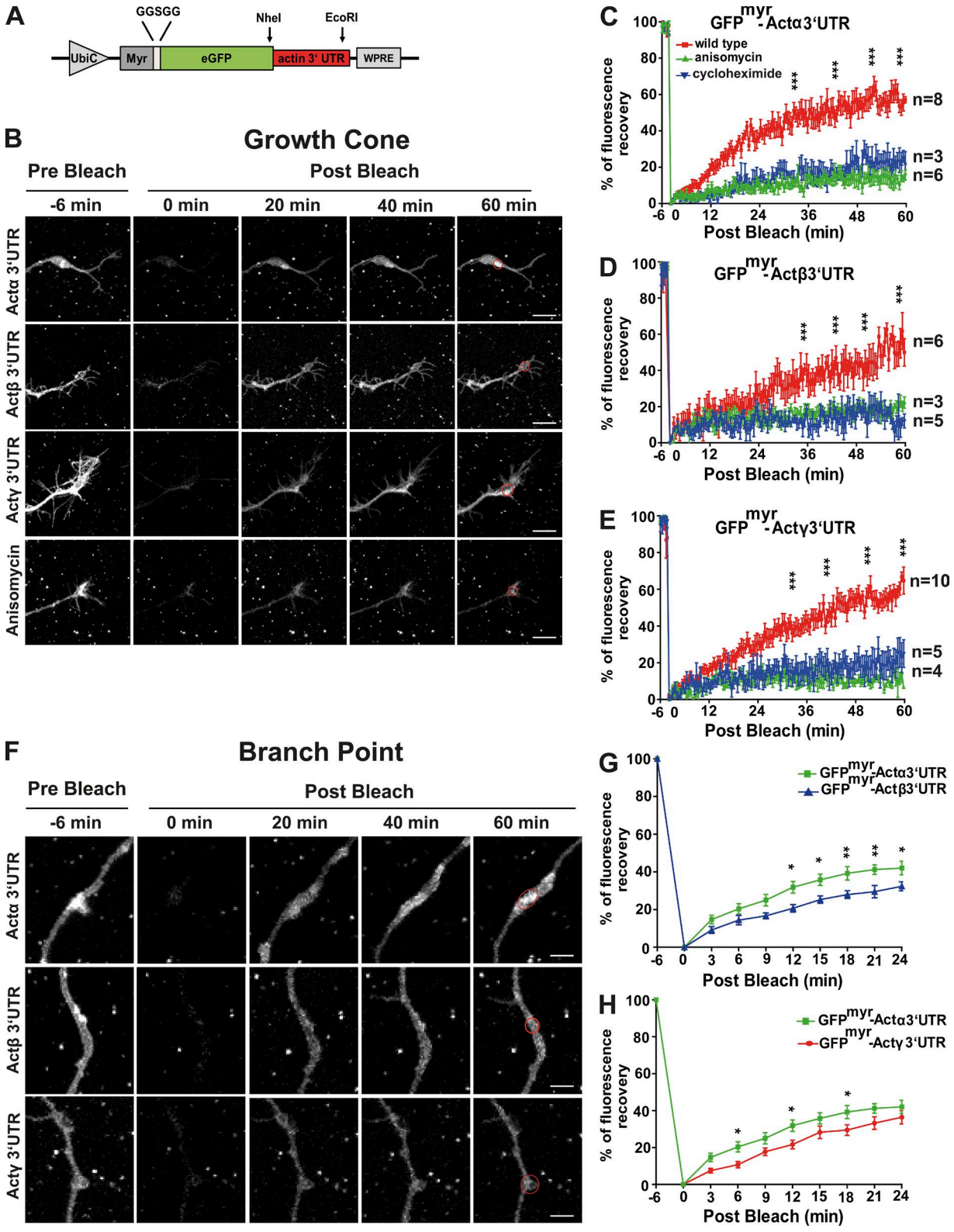

Figure 4. **3′ UTRs of Actα, Actβ, and Actγ drive local translation of reporter mRNAs in axonal growth cones and branch points.** (A) Scheme of reporter constructs with coding sequence of myristoylated eGFP and respective 3′ UTRs of actin isoforms. (B) Representative time-lapse images from FRAP in growth cones of eGFP^{myr}-3′ UTR–expressing motoneurons. eGFP^{myr} was bleached and fluorescence recovery was monitored in defined regions of interest within the growth cone indicated in red circles. Quantification of FRAP shows 60% recovery of fluorescence signals in growth cones of motoneurons expressing eGFP^{myr}-3′ UTR of Actα (C), eGFP^{myr}-3′ UTR of Actβ (D), and eGFP^{myr}-3′ UTR of Actγ (E), and recovery is decreased after anisomycin and cycloheximide treatments (***, $P < 0.001$). (F) Representative time-lapse images of FRAP sequences of branch points in the distal axon. (G and H) Quantification of FRAP in defined ROIs within branch points (indicted in red circles) shows a faster recovery for eGFP^{myr}-3′ UTR of Actα in the first 20 min after bleach compared with eGFP^{myr}-3′ UTR of Actβ (*, $P < 0.05$; **, $P < 0.01$) and eGFP^{myr}-3′ UTR of Actγ (*, $P < 0.05$). Statistical analysis was performed by two-way ANOVA with Bonferroni post hoc test. Bar, 10 µm.

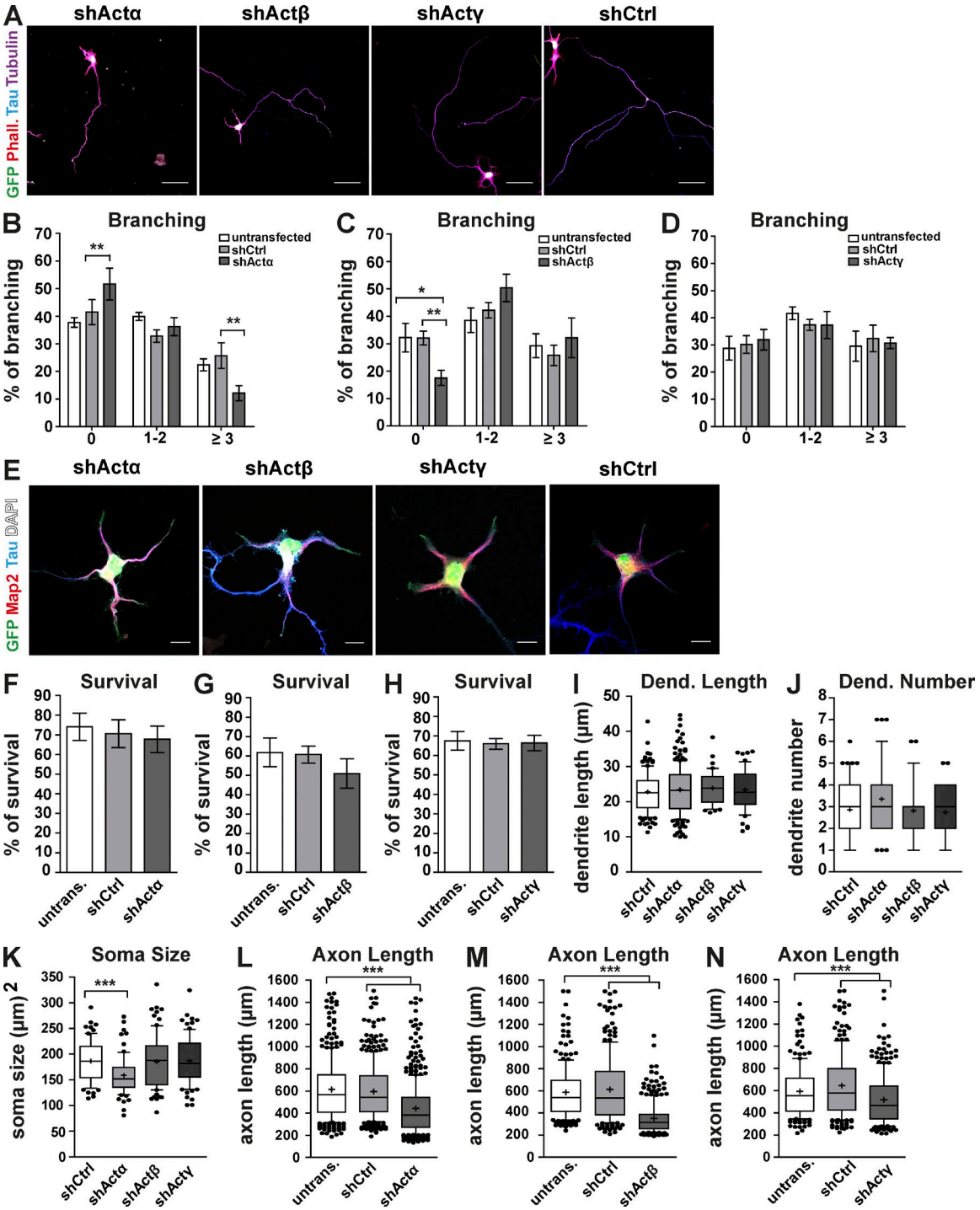

Figure 5. **Actα promotes formation of axonal collateral branches in motoneurons.** (A) Motoneurons were transduced with lentivirus expressing shRNA targeting 3′ UTRs of actin isoforms. Immunostaining with phalloidin and against Tau and tubulin labels axons and mature branches. GFP is coexpressed with shRNAs to label transduced cells. (B) In Actα-depleted neurons, the number of axons without collateral branches increases, and the number of axons with three or more branches decreases (**, $P < 0.01$ for $n = 5$). (C) Knockdown of Actβ increases number of axonal collateral branches (*, $P < 0.031$; **, $P < 0.01$ for $n = 6$). (D) Depletion of Actγ does not affect branch formation ($n = 4$). Statistical analysis was performed using two-way ANOVA with Bonferroni post hoc test. (E) Dendrites are immunolabeled against Tau and Map2. (F–H) Motoneuron viability is not affected by knockdown of actin isoforms (F: $n = 6$; G and H: $n = 5$). Dendrite length (I) and number (J) are not altered by knockdown of individual actin isoforms ($n = 5$; sample size: I: shActα: 190, shActβ: 116, shActγ: 149, shCtrl: 136; J: shActα: 58, shActβ: 38, shActγ: 46, shCtrl: 49 cells). (K) Knockdown of Actα causes a reduction in soma size, whereas knockdown of Actβ and Actγ does not affect soma growth (***, $P < 0.0001$ for $n = 5$; sample size: shActα: 76, shActβ: 82, shActγ: 83, shCtrl: 69 cells). (L–N) Axon length is reduced after knockdown of Actα, Actβ, or Actγ (L: ***, $P < 0.0001$ for $n = 5$; sample size: shActα: 452, shCtrl: 380, untransduced: 328; M: ***, $P < 0.0001$ for $n = 5$; sample size: shActβ: 279, shCtrl: 227, untransduced: 219; N: ***, $P < 0.0001$ for $n = 4$; sample size: shActγ: 252, shCtrl: 228, untransduced: 180 cells). Statistical analysis in F–N was performed by one-way ANOVA with Dunn's post-test. In B–H, data are shown as mean ± SEM. Bars: (A) 50 µm; (E) 10 µm.

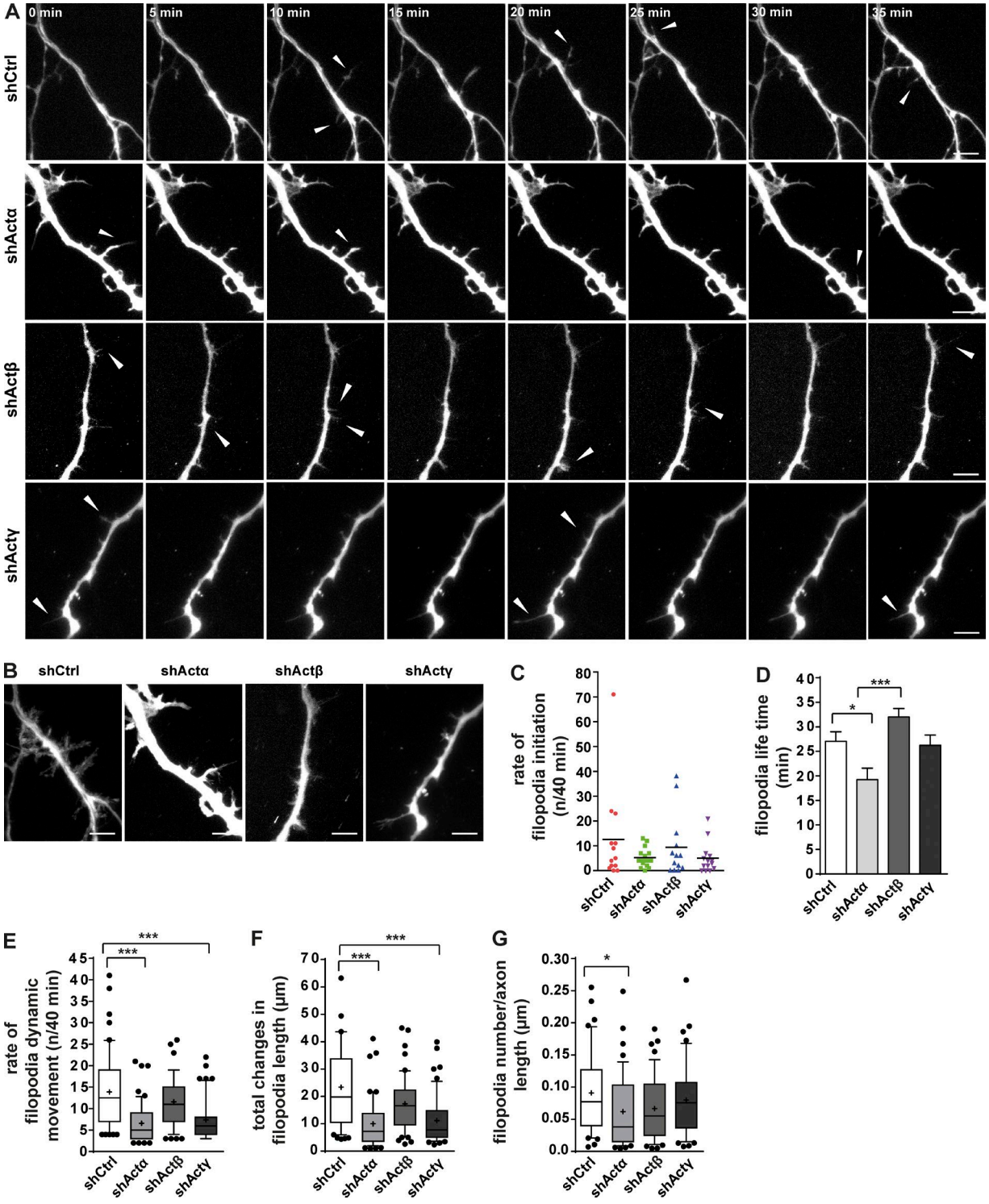

Figure 6. **Dynamics of axonal filopodia are reduced in Actα and Actγ knockdown motoneurons.** (A) Time-lapse sequences representing axonal filopodia dynamics in motoneurons transduced with actin knockdown lentiviruses coexpressing GFP (Videos 1–4). Arrowheads mark dynamic filopodia. (B) Maximum projection of 120 frames representing alterations in filopodia length over time. (C) Rate of filopodia initiation is decreased by 60% after Actα or Actγ knockdown. (D) Lifetime of Actα-depleted filopodia is decreased compared with control (*, $P < 0.010$) and Actβ-depleted filopodia (***, $P < 0.0008$). Shown are mean ± SEM. (E) Graph shows mean rate of filopodia dynamic movement. Rate of filopodia movement is decreased in Actα- and Actγ-depleted neurons. (F) Graph showing mean total changes in filopodia length. Filopodia growth dynamics is reduced after Actα and Actγ knockdown (E and F: ***, $P < 0.0001$, shActα: $n = 4$, shActβ: $n = 5$, shActγ: $n = 3$, shCtrl: $n = 6$ for 50 filopodia per group). (G) Motoneurons were stained with phalloidin, and filopodia were counted per micrometer of axon length. Depletion of Actα reduces number of axonal filopodia (*, $P < 0.043$). Statistical analysis was performed using one-way ANOVA with Dunn's post-test. Bars, 5 µm.

suggest that Actα and Actγ, but not Actβ, modulate the dynamics of axonal filopodia.

This finding was surprising on the basis of previous works that emphasized the importance of locally synthesized Actβ for axon guidance (Leung et al., 2006) and elongation (Rossoll et al., 2003). In our study, we also observed impaired axonal growth in Actβ-depleted motoneurons (Fig. 5 M). Nevertheless, this phenotype was not specific for Actβ, because we also observed shorter axons in Actα- and Actγ-depleted neurons. Therefore, we investigated the maturation and dynamics of axonal growth cones in Actβ knockdown motoneurons. First, we analyzed the growth cone size of DIV5 motoneurons by phalloidin staining (Fig. 7 A). We cultured motoneurons on a synapse-specific laminin (laminin 221), as this matrix protein induces maturation of growth cones and formation of presynaptic structures in cultured motoneurons (Porter et al., 1995; Jablonka et al., 2007). Interestingly, we observed 50% reduction in axonal growth cone size and number of growth cone filopodia ($P < 0.0001$) after depletion of Actβ, whereas Actα- and Actγ-depleted neurons could form normal growth cones (Fig. 7, B and C). Next, we investigated the dynamics of growth cone motility using time lapse imaging. We monitored growth cone movements of actin isoform–specific knockdown motoneurons for 40 min (Fig. 7 D) and analyzed the velocity of filopodia and lamellipodia movements by creating multiple kymographs (Fig. 7, E–H). Interestingly, we observed 50% reduction in growth cone movement velocity of Actβ-depleted neurons ($P < 0.0001$; Fig. 7 I and Videos 5 and 7), whereas depletion of Actα and Actγ had no effect (Fig. 7 I and Videos 6 and 8). Reduced growth cone size and motility upon Actβ depletion suggests a specific function for this isoform in axon pathfinding and differentiation of growth cones into functional synapses. Collectively, these data indicate that each actin isoform accomplishes a distinct function in motoneuron growth and differentiation.

Lack of Actβ is partially compensated by elevated expression of Actα and Actγ

We then asked whether Actα and Actγ isoforms could compensate for Actβ loss in motoneurons. To address this question, we quantified filamentous actin in Actβ-depleted motoneurons in the soma and axon by phalloidin staining (Fig. 8 A). Upon Actβ depletion, phalloidin intensity was not altered in the soma (Fig. 8 B), whereas it was highly reduced in the axon ($P < 0.0001$; Fig. 8 C). Notably, knockdown of Actα or Actγ had no effect on F-actin levels in the soma either (Fig. 8 B), indicating that actin isoforms are functionally redundant in this compartment. Nevertheless, in the axon, similar to Actβ, depletion of Actα impaired F-actin levels ($P < 0.0018$; Fig. 8 C). These data refer to an important role of both Actα and Actβ in actin dynamics, particularly in the axon. Furthermore, we performed Western blot analysis to measure the total actin levels in protein lysates of cultured motoneurons in which individual actin isoforms had been suppressed by lentiviral shRNAs. As shown in Fig. 8 (D and E), the levels of total actin remained constant in Actα-, Actβ-, or Actγ-depleted motoneurons. Next, we investigated the G- to F-actin ratio by ultracentrifugation of the lysates and probed the separated G- and F-actin pools with pan–actin antibody (Fig. 8 F). Knockdown of Actα, Actβ, or Actγ did not cause any significant shift in the G- to F-actin ratio, indicating that these isoforms can act redundantly and thus compensate for each other's loss (Fig. 8 G). We also investigated the G- to F-actin ratio using Actβ-specific antibody (Fig. 8 H). Interestingly, knockdown of either Actα or Actγ resulted in increased levels of Actβ in the G-actin pool and decreased levels in the F-actin pool ($P < 0.016$; Fig. 8 I). These data indicate that polymerization and/or stabilization of Actβ-containing filaments depends on Actα and Actγ. Maintenance of the total actin levels after depletion of each actin isoform might refer to a compensatory up-regulation of other isoforms. To assess this possibility, we analyzed mRNA levels of these isoforms by quantitative RT-PCR and found that after depletion of Actα, the expression of Actβ or Actγ did not change (Fig. 9 A); however, the mRNA levels of these two isoforms were increased in the axon ($P < 0.011$; Fig. 9 D). Depletion of Actβ led to a 5.5-fold increase in total Actα mRNA levels ($P < 0.0005$) and a 2.6-fold increase in total Actγ mRNA levels ($P < 0.018$; Fig. 9 B). Actα and Actγ mRNA levels were also increased in the axonal compartment of Actβ-depleted motoneurons ($P < 0.014$; Fig. 9 E). Similarly, knockdown of Actγ led to a 1.6-fold increase in Actα and a 2.6-fold increase in Actβ total mRNA levels ($P < 0.0054$; Fig. 9 C). Also in the axonal compartment, depletion of Actγ led to a 2.5-fold increase in Actα mRNA levels ($P < 0.002$; Fig. 9 F). Next, we asked whether such compensatory up-regulation of mRNA of these isoforms corresponds to an increment in their protein levels. Western blot analysis of lysates obtained from Actβ-depleted motoneurons showed a 2.5-fold increase in Actα protein levels ($P < 0.004$; Fig. 9, G and J). Likewise, Actβ protein levels were increased in lysates of Actγ knockdown motoneurons ($P < 0.0003$; Fig. 9, H and K) and Actγ protein levels were increased in lysates of Actβ knockdown motoneurons ($P < 0.002$; Fig. 9, I and L). Altogether, these results confirm that depletion of Actβ isoform initiates a compensatory response in motoneurons that results in up-regulation of both Actα and Actγ isoforms.

Axonal mRNA trafficking and translation of actin isoforms are impaired in Smn-deficient motoneurons

In previous studies, we have reported that both axonal localization and translation of Actβ mRNA are impaired in Smn-deficient motoneurons (Rathod et al., 2012). We now asked whether Smn deficiency could also affect the axonal mRNA transport of Actα and Actγ isoforms. Thus, we investigated mRNA expression of actin isoforms in the soma and axon of Smn knockdown motoneurons by quantitative RT-PCR (Fig. 10, A–C). We found that in the somatodendritic compartment, mRNA levels of all three actin isoforms were not altered (Fig. 10 B), whereas mRNA levels of all three isoforms were significantly reduced in the axonal compartment ($P < 0.021$ for Actα and $P < 0.013$ for Actβ and Actγ; Fig. 10 C). These results indicate that Smn protein is involved in the axonal translocation of the transcripts for all three actin isoforms. Moreover, we assessed the role of Smn in regulation of the local translation of actin isoforms in growth cones by FRAP experiments. We observed a significant reduction in the fluorescence recovery of Actα ($P < 0.001$), Actβ ($P < 0.01$), and Actγ reporters ($P < 0.05$) in motoneurons isolated from type I SMA mice, indicating that Smn is required for the local translation of actin isoforms in the axonal growth cone (Fig. 10, D–F). Nevertheless, this delayed recovery might also be caused by decreased levels of Actα, Actβ, and Actγ mRNAs in the distal axon of Smn-deficient motoneurons (Fig. 10 C).

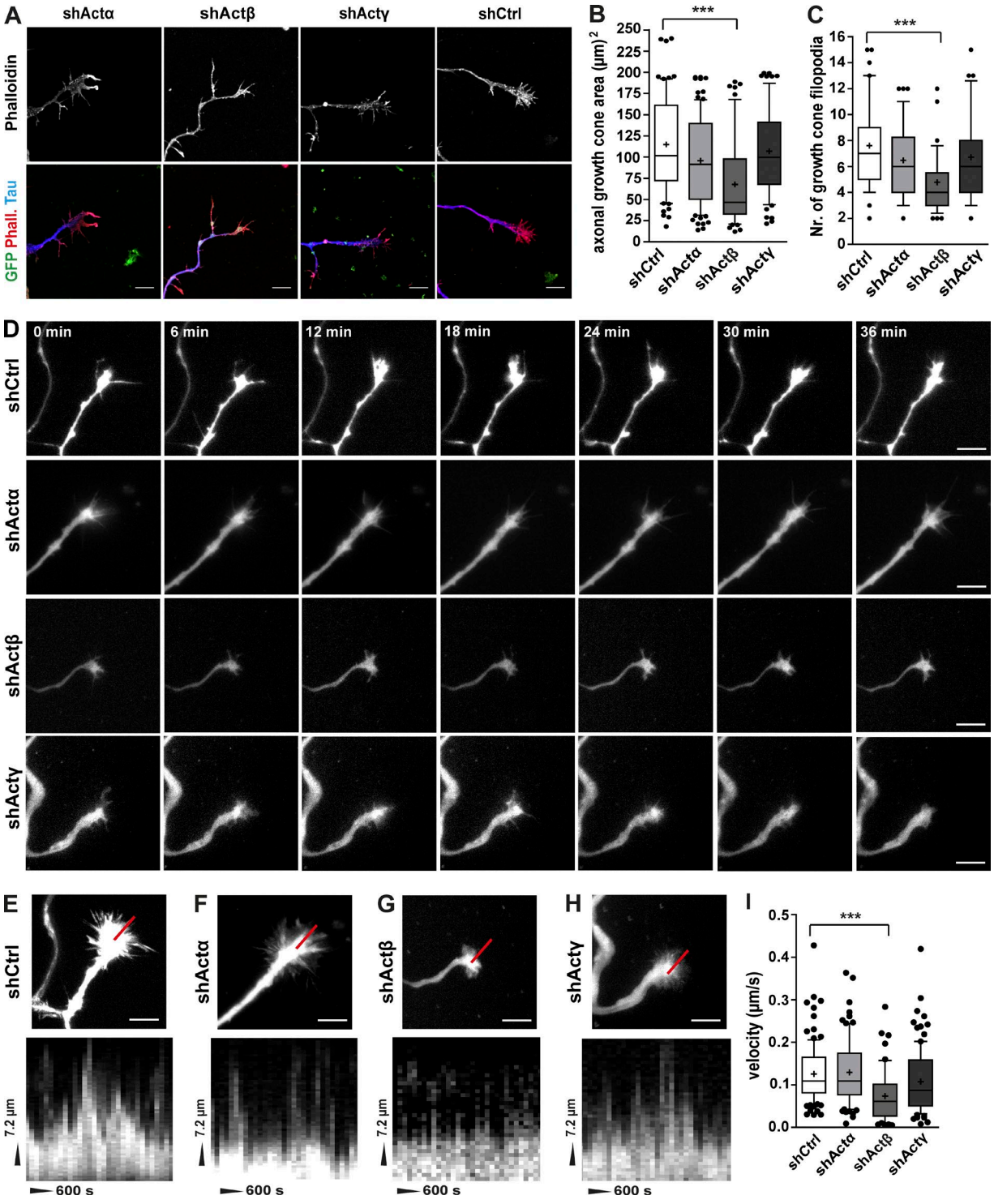

Figure 7. **Actβ-depleted motoneurons show smaller growth cones and reduced growth cone motility.** (A) Motoneurons were transduced with shRNA expressing lentiviruses targeting actin isoforms and plated on laminin 221. Cells were fixed at DIV5 and stained with phalloidin and against Tau. Bars, 10 µm. (B and C) Growth cone area (B) and number of growth cone filopodia (C) are reduced after knockdown of Actβ (***, $P < 0.0001$ for $n = 6$; sample size: shActα: 96, shActβ: 54, shActγ: 67, shCtrl: 70 cells). (D) Time-lapse images representing dynamics of filopodia in growth cones of actin isoform–specific knockdown motoneurons (Videos 5–8). (E–H) Top panel shows maximum projection of 120 time-lapse images for measuring total changes in axonal growth cone movement in shCtrl (E), shActα (F), shActβ (G), and shActγ (H) transduced motoneurons, and lower panel shows multiple kymographs representing changes in filopodia/lamellipodia length (µm) over 10 min (time shown in seconds) along the red line inserted above. (I) Knockdown of Actβ reduces velocity of growth cone movements (***, $P < 0.0001$ for $n = 3$; sample size: shActα: 17, shActβ: 16, shActγ: 13, shCtrl: 15 cells). Statistical analysis was performed using one-way ANOVA with Dunn's post-test. Bars: (D–H) 5 µm.

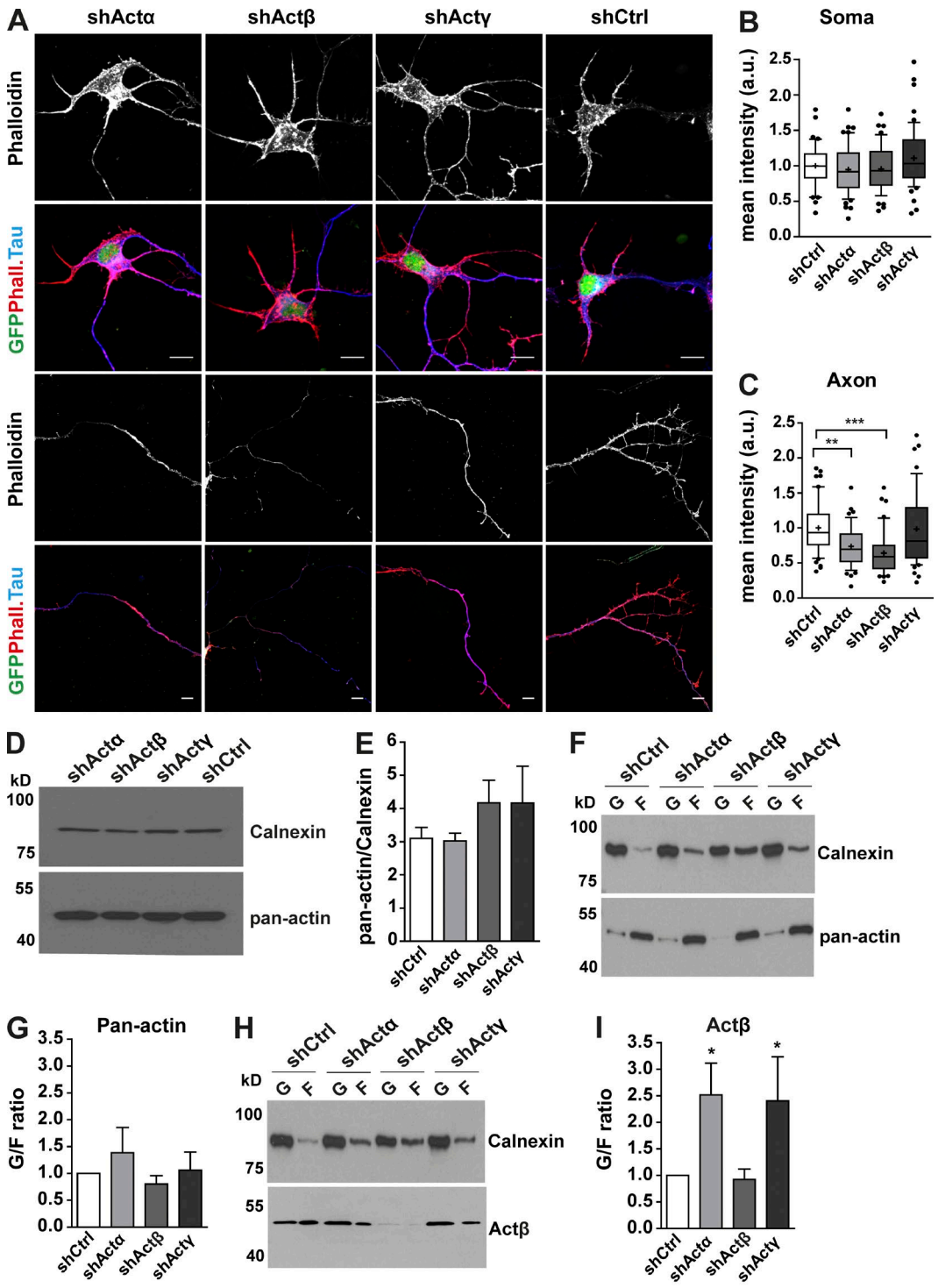

Figure 8. **Depletion of Actα and Actβ affects F-actin polymerization in axons.** (A) Motoneurons transduced with respective shRNAs against actin isoforms were fixed and stained with phalloidin and against Tau. Mean intensity of phalloidin staining was measured and normalized to mean intensity of phalloidin in shCtrl group. (B) In the soma, phalloidin intensity is not altered ($P < 0.208$ for $n = 3$; sample size: shActα: 55, shActβ: 47, shActγ: 53, shCtrl: 44 cells). (C) Phalloidin intensity is reduced in axons after knockdown of Actα and Actβ (**, $P < 0.0018$ for shActα; ***, $P < 0.0001$ for shActβ for $n = 3$; sample size: shActα: 48, shActβ: 46, shActγ: 53, shCtrl: 54 cells). Bars, 10 µm. (D) Western blot analysis of lysates from actin isoform–specific knockdown motoneuron cultures probed with pan–actin antibody ($n = 4$). (E) Total actin levels remain constant after depletion of each actin isoform. (F) Immunoblots of supernatant (G-actin) and pellet fractions (F-actin) of motoneuron lysates after ultracentrifugation probed with pan–actin antibody. (G) Quantification shows no change in the G- to F-actin ratio after depletion of individual actin isoforms ($n = 5$). (H) Supernatant and pellet fractions of motoneuron lysates were labeled with Actβ antibody. (I) Quantification of the G- to F-actin ratio shows increased levels of Actβ in the G-actin pool after knockdown of Actα and Actγ (*, $P < 0.016$ for $n = 5$). Statistical analysis was done using one-way ANOVA with Dunn's post-test (B–E) or one-tailed Mann–Whitney test (G and I). In E–I, data are shown as mean ± SEM.

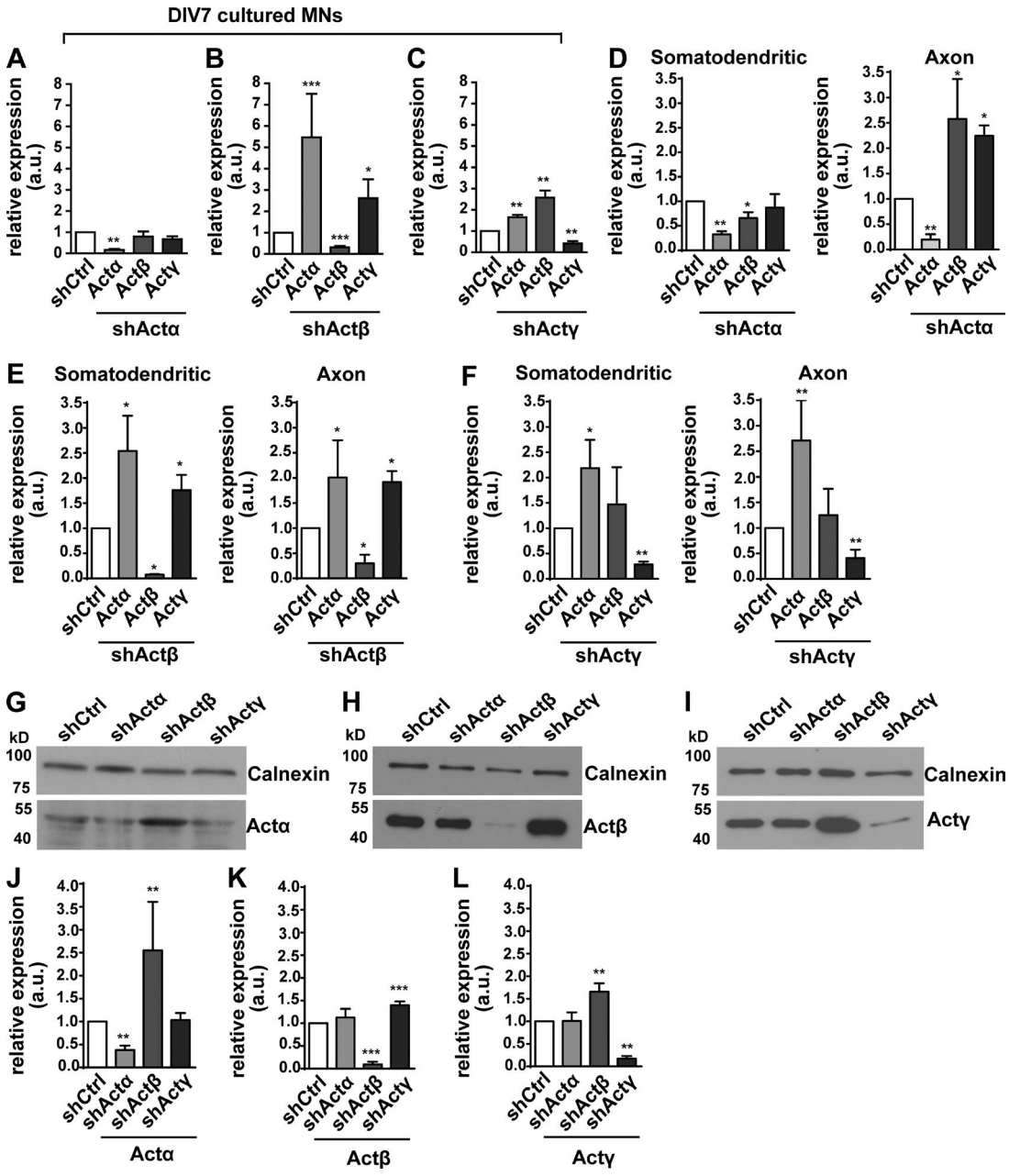

Figure 9. **Compensatory regulation of actin isoforms in the somatodendritic and axonal compartments after depletion of Actα, Actβ, or Actγ.** (A–C) RNA was prepared from actin knockdown and control motoneuron cultures and analyzed by quantitative RT-PCR. (A) mRNA levels of Actα are decreased after shRNA-mediated knockdown, whereas mRNA levels of Actβ and Actγ are not altered (**, $P < 0.0037$ for $n = 5$). (B) Depletion of Actβ leads to a 70% decrease in Actβ (***, $P < 0.0005$), a 5.5-fold increase in Actα (***, $P < 0.0005$), and a 2.6-fold increase in Actγ mRNA levels (*, $P < 0.018$ for $n = 7$). (C) Depletion of Actγ leads to a 80% decrease in Actγ (**, $P < 0.001$), a 1.6-fold increase in Actα, and a 2.6-fold increase in Actβ mRNA levels (**, $P < 0.0054$ for $n = 5$). (D–F) Quantitative RT-PCR analysis of RNA samples obtained from somatodendritic and axonal compartments of motoneuron cultures transduced with actin shRNA constructs. (D) In Actα-depleted motoneurons, mRNA levels of Actα are decreased in both somatodendritic and axonal compartments (**, $P < 0.002$), mRNA levels of Actβ are decreased in the somatodendritic compartment (* $P < 0.047$) and mRNA levels of both Actβ and Actγ are increased in the axonal compartment (*, $P < 0.011$ for $n = 5$). (E) In Actβ-depleted motoneurons, mRNA levels of Actβ are decreased in somatodendritic and axonal compartments (*, $P < 0.014$) and mRNA levels of Actα and Actγ are increased in both somatodendritic (*, $P < 0.028$) and axonal compartments (*, $P < 0.014$ for $n = 4$). (F) In Actγ-depleted motoneurons, mRNA levels of Actγ are decreased in somatodendritic (**, $P < 0.002$) and axonal compartments (**, $P < 0.001$) and mRNA levels of Actα are increased in somatodendritic (*, $P < 0.046$) and axonal compartments (**, $P < 0.002$ for $n = 5$). (G–I) Western blot analysis of cultured motoneuron lysates probed with specific Actα (G), Actβ (H), and Actγ (I) antibodies. (J) Quantification of blots in G showed 2.5-fold up-regulation of Actα protein after knockdown of Actβ (**, $P < 0.004$ for $n = 4$). (K) Quantification of blots in H showed 1.5-fold up-regulation of Actβ protein after knockdown of Actγ (***, $P < 0.0003$ for $n = 8$). (L) Quantification of blots in I showed 1.7-fold up-regulation of Actγ protein after knockdown of Actβ (**, $P < 0.002$ for $n = 6$). Statistical analysis was performed using a one-tailed Mann-Whitney test. Shown are mean ± SEM.

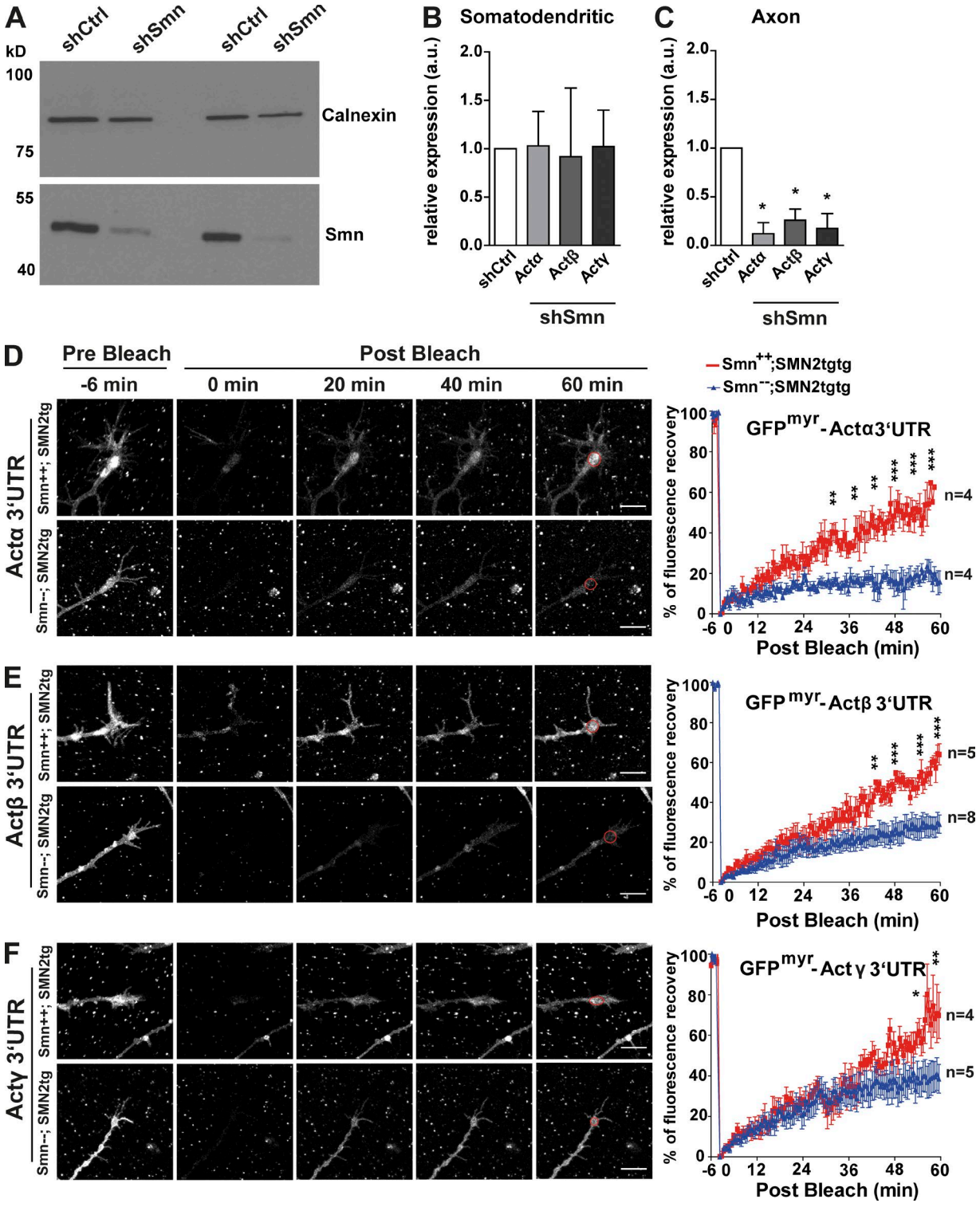

Figure 10. **Axonal transport and translation of Actα, Actβ, and Actγ mRNAs are impaired in Smn-deficient motoneurons.** (A) Immunoblot shows reduction in Smn protein levels in motoneuron lysates after shRNA-mediated knockdown of Smn. Calnexin was used as loading control. A Western blot from two independent knockdown experiments is shown (representative for $n = 3$). (B) shSmn transduced motoneurons were plated in microfluidic chambers, and RNA was extracted and analyzed by quantitative RT-PCR. mRNA levels of actin isoforms are not altered in the somatodendritic compartment. (C) Axonal mRNA levels of all three actin isoforms are reduced in Smn-depleted neurons (*, $P < 0.021$ for Actα; *, $P < 0.013$ for Actβ and Actγ for $n = 4$). Statistical analysis was done using a one-tailed Mann-Whitney test. (D–F) On the left are representative time-lapse images of FRAP sequences of growth cones of motoneurons isolated from type I SMA mice transduced with eGFP^{myr}-Actα3′UTR (D), eGFP^{myr}-Actβ3′UTR (E), and eGFP^{myr}-Actγ3′UTR (F). (D) The graph on the right shows a reduction in fluorescence recovery of Actα reporter in *Smn^{--}; SMN2tgtg* compared with *Smn^{++}; SMN2tgtg* neurons (**, $P < 0.01$; ***, $P < 0.001$). (E, right) Fluorescence recovery of Actβ reporter is reduced in Smn-deficient neurons (**, $P < 0.01$; ***, $P < 0.001$). ROIs are indicated in red circles. (F, right) Differences in recovery of Actγ reporter become apparent after 54 min after bleach (*, $P < 0.05$; **, $P < 0.01$). Statistical analysis in D–F was done using a two-way ANOVA with Bonferroni post hoc test. Shown are mean ± SEM. Bars, 10 µm.

Discussion

In the present study, we observed that Actα, Actβ, and Actγ isoforms accomplish specific functions in axon growth and differentiation in motoneurons. All three actin isoforms are expressed in motoneurons, and their mRNAs are transported into distal axons, indicating that in addition to Actβ, intra-axonal protein synthesis of Actα and Actγ contributes to differential regulation of motor axon growth and maturation. Motoneurons appear unique in this aspect, because the levels of Actα are much lower in the axonal compartment of cortical neurons (Fig. S5). Thus, developing motoneurons differ from other types of neurons reported previously to contain only mRNAs for Actβ in the axon (Bassell et al., 1998; Zheng et al., 2001; Willis et al., 2007; Minis et al., 2014). Of note, in differentiating myoblasts, mRNAs for Actβ localize to the leading lamellae and mRNAs for Actα localize to perinuclear compartments (Taneja and Singer, 1990; Kislauskis et al., 1993). In cultured cerebrocortical neurons, mRNA for Actβ is present in axons and growth cones, whereas mRNA for Actγ is not enriched in axons (Bassell et al., 1998). Also in sensory neurons, GFP mRNA containing the 3′ UTR of Actβ translocates into axons, whereas the 3′ UTR of Actγ cannot drive the transport of GFP mRNA into axons (Willis et al., 2007, 2011; Donnelly et al., 2011). However, in more recent studies using sensitive techniques, mRNAs for Actγ could be detected in hippocampal synapse–enriched fractions, and mRNAs for both Actα and Actγ were detected in neuropil and somata layers of the CA1 region of the hippocampus (Cajigas et al., 2012; Schreiber et al., 2015).

Knockout mouse models for the different actin isoforms have provided evidence both for their specific and overlapping cellular functions. Ablation of Actβ from mouse embryonic fibroblasts impairs cell division and migration, functions that correlate with altered G- to F-actin ratio and gene expression (Dugina et al., 2009; Bunnell et al., 2011). Nevertheless, impaired migration of these fibroblasts can be restored by Actα and Actγ if ROCK signaling pathway is inhibited, suggesting that these actin isoforms can act redundantly (Tondeleir et al., 2012). CNS-specific ablation of Actβ causes perturbations in the morphology of the cerebellum and hippocampus that correlate with neuronal hyperactivity, poor cognitive performance, and altered maternal behavior (Cheever et al., 2012). Also, knockout mouse models for Actα exhibit distinct phenotypes such as growth defects, muscle weakness, and heart defects. These mice die at early postnatal stages (Schildmeyer et al., 2000; Crawford et al., 2002). In humans, point mutations in skeletal Actα gene lead to congenital nemaline myopathy associated with pronounced muscle weakness and hypotonia (Nowak et al., 1999; Ohlsson et al., 2004; Wallgren-Pettersson et al., 2004). Actγ knockout mice are viable but exhibit developmental delays and reduced survival, progressive muscle necrosis, myopathy, and deafness (Sonnemann et al., 2006; Belyantseva et al., 2009). Also, fibroblasts lacking Actγ show reduced viability, impaired growth, and reduced migration capacity (Dugina et al., 2009; Bunnell and Ervasti, 2010). Moreover, conditional knockout of Actγ in hippocampus causes increased fear memory consolidation, indicating a role of this isoform in memory formation (Schreiber et al., 2015). Interestingly, in all these mouse models, a compensatory up-regulation of the remaining actin isoforms is observed. Actβ knockout mice exhibit up-regulation of Actα and Actγ (Bunnell et al., 2011; Cheever et al., 2012; Tondeleir et al., 2012). In Actγ knockout mice and Actγ-depleted fibroblasts, Actα and Actβ are up-regulated (Belyantseva et al., 2009; Dugina et al., 2009; Bunnell and Ervasti, 2010; Schreiber et al., 2015). Likewise, knockout of cardiac Actα leads to compensatory up-regulation of skeletal muscle Actα (Kumar et al., 2004). Knockout of skeletal muscle Actα increases the expression of both vascular and cardiac Actα isoforms (Crawford et al., 2002), and knockout of smooth muscle Actα leads to up-regulation of skeletal muscle Actα (Schildmeyer et al., 2000). Intriguingly, in some of these actin isoform–specific knockout mice, the phenotype is fully rescued by transgenic overexpression of other isoforms (Perrin and Ervasti, 2010). Overexpression of cardiac Actα in knockout mouse models of skeletal muscle Actα rescues the lethality and improves muscle performance (Nowak et al., 2009). Overexpression of smooth muscle Actγ only partially rescues the heart defects in cardiac Actα knockout mice (Kumar et al., 1997), and overexpression of Actγ does not rescue the lethality of skeletal muscle Actα knockout mice (Jaeger et al., 2009). These observations indicate that some actin isoforms can functionally substitute other isoforms. In our study, we also observed an up-regulation of Actα and Actγ in Actβ-depleted motoneurons and up-regulation of Actα and Actβ in Actγ-depleted motoneurons so that the levels of total actin were maintained. Consistent with this, Actα and Actγ could compensate for the loss of Actβ and preserve the F-actin polymerization capacity in the soma and maintain the G- to F-actin ratio. Moreover, we observed enhanced axonal branch formation in Actβ-depleted neurons, which could be a consequence of Actα up-regulation. However, defects in axonal elongation and growth cone maturation observed in Actβ-depleted neurons could not be fully rescued in vitro. In contrast, in vivo studies using a motoneuron-specific Actβ conditional knockout mouse model have shown that loss of function of this isoform does not lead to functional and morphological motor deficits (Cheever et al., 2011). This indicates that in motoneurons, Actα and Actγ can compensate for Actβ deficiency in vivo and thus completely rescue the loss of this isoform.

Functional differences between actin isoforms are mostly caused by sequence differences in their N termini, which allow them acquire diverse chemical and physical properties. Actin filaments composed primarily of Actα show very high viscoelasticity and can form highly elastic gels, whereas filaments with Actγ form less elastic structures, and filaments with Actβ cannot form elastic gels (Allen et al., 1996). The phalloidin-binding affinity is twofold higher for Actβ than for Actα, and the ATP hydrolysis of Actβ, in contrast to Actα monomers, happens before polymerization (Nyman et al., 2002). These differences in physical properties directly translate into unique polymerization kinetics of actin isoforms. Polymers with high ratio of Actβ are highly dynamic and depolymerize rapidly, whereas incorporation of Actα or Actγ slows down the turnover rate of actin filaments and stabilizes them (Bergeron et al., 2010). The lower turnover of actin filaments that include Actα could also be explained by discriminative binding of actin regulatory proteins to specific isoforms, as both profilin and cofilin show higher binding affinities to Actβ monomer/filaments than to Actα (Larsson and Lindberg, 1988; De La Cruz, 2005). Thus, differences in polymerization kinetics of actin isoforms may reflect differences in their cellular functions. In line with these previous data, we found that depletion of Actα or Actγ causes a shift in the G- to F-actin ratio of Actβ and thus results in increased amounts of Actβ in the G-actin pool. These results show that the stability of Actβ-containing filaments is determined by Actα and Actγ. Interestingly, although

knockdown of all three actin isoforms impaired axon elongation, depletion of Actβ had a more prominent effect on this process compared with the other two isoforms. This phenotype could be explained by elevated levels of Actα and Actγ observed in Actβ-depleted motoneurons, which might reduce the turnover of the actin filaments in the axon and stabilize the cytoskeleton to such an extent that this favors reduced growth cone movements and reduced axonal elongation. Hence, a balance between dynamic and stability of the actin cytoskeleton in the axon appears to be crucial for proper axon growth in neurons. Also in hippocampal dendrites, increased synaptic protein levels of Actγ increases spine density and enhances short-term contextual fear memory (Schreiber et al., 2015). In this cellular compartment, incorporation of Actγ into actin filaments apparently increases F-actin stability and thus influences spine morphology.

In contrast to the axonal growth cone, the axon shaft shows relatively low protrusive activity (Letourneau, 2009). In sensory neurons, actin polymerization rate is different in growth cone filopodia and axonal filopodia, as a 5-min NGF pulse rapidly increases the number of growth cone filopodia, whereas the increase in the axonal filopodia is delayed and occurs only after 30-min NGF treatment (Spillane et al., 2012). Using live-cell imaging, we observed that the dynamics of axonal filopodia extension/retraction are much lower than those of the axonal growth cone filopodia, indicating that actin polymerization differs in these two subcellular compartments. Also, our immunofluorescence experiments show that Actα predominantly localizes to axonal branch points, whereas Actβ is highly enriched in the growth cone filopodia and Actγ in axonal filopodia. Consistent with this, we found that knockdown of Actα or Actγ reduces the dynamics of axonal filopodia, whereas depletion of Actβ only impairs growth cone dynamic movements and prevents maturation of the growth cone. These observations, together with the fact that cofilin/actin-depolimerizing factor has a lower binding affinity to Actα, suggest that Actα and Actγ contribute to polymerization of a stable F-actin in the axonal filopodia and Actβ contributes to polymerization of dynamic F-actin in growth cone filopodia and lamellipodia.

After spinal cord lesion in adult rats, application of antibodies against the growth inhibitory protein Nogo-A leads to enhanced sprouting in corticospinal tract (Z'Graggen et al., 1998; Chen et al., 2000; Blöchlinger et al., 2001; Bareyre et al., 2002; Schwab, 2004). The observed compensatory sprouting is associated with up-regulation of growth factors such brain-derived neurotrophic factor (BDNF), GAP-43, and myosin. However, a relatively high up-regulation of Actα was also observed in these studies (Bareyre et al., 2002). Intra-axonal protein synthesis is required for axon sprouting in vivo (McWhorter et al., 2003; Qiu et al., 2009; Buckmaster and Wen, 2011), and diverse cytoskeletal proteins, including Actβ, subunits of the Arp2/3 complex, WAVE1, and the complex stabilizer cortactin are locally translated at branch points in vitro (Spillane et al., 2012, 2013). In isolated embryonic motoneurons, we found that Actα protein is highly enriched in the axonal branch points and the rate of its local translation is much faster than for Actβ and Actγ at branch points. Interestingly, ablation of Actα disturbs formation of axonal collateral branches. Thus, the positive effects of antibodies against Nogo-A on axon regeneration might involve mechanisms for increased expression and axonal transport of Actα, allowing formation of highly stable actin filaments and thereby stabilizing transiently formed sprouts.

Studies on type I mouse models of SMA have revealed that motoneurons isolated from these mice display defects in axon elongation and growth cone formation (Rossoll et al., 2003; Ning et al., 2010). Furthermore, Smn knockout mice show altered clustering of voltage-gated Ca^{2+} channels in the growth cone, impaired maturation of neuromuscular endplates and neurotransmitter release, and severe neuromuscular denervation (Jablonka et al., 2007; Kariya et al., 2008; Kong et al., 2009; Ling et al., 2012). Both in mild SMA patients and in type III SMA mouse models, enhanced axonal sprouting is observed that provides a compensatory mechanism for remaining intact motor axons to reinnervate the denervated muscle fibers and thus modulate muscle weakness in SMA patients (Crawford and Pardo, 1996; Simon et al., 2010). However, this compensatory sprouting is not observed in severe SMA patients and in type I SMA mouse models (Cifuentes-Diaz et al., 2002; Murray et al., 2008). Thus, therapeutic strategies that promote axonal growth and sprouting could improve synaptic innervation and attenuate disease phenotype in severe SMA patients (Bosch-Marcé et al., 2011). Notably, we found that depletion of Smn protein impairs both axonal translocation and translation of all three actin isoforms. Thus, mislocalization of Actα and Actβ mRNAs could account for the lack of sprouting and defective active zone formation, respectively, in Smn-deficient motoneurons and thus could explain why these cells are predominantly affected in SMA patients. Amyotrophic lateral sclerosis (ALS) is another motoneuron disease characterized by degeneration of upper and lower motoneurons, muscle weakness, and atrophy and death from respiratory failure (Andersen and Al-Chalabi, 2011; Ferraiuolo et al., 2011). In familial ALS patients, autosomal-dominant mutations in several genes have been reported (Ferraiuolo et al., 2011). Interestingly, microarray and quantitative RT-PCR assays have shown that the expression of Actγ increases in sporadic ALS patients (Baciu et al., 2012). Presuming that Actγ contributes to actin filaments with lower turnover (Bergeron et al., 2010), its up-regulation in ALS patients might represent a compensatory mechanism for actin cytoskeleton stabilization in mature axons, thereby modulating axon maintenance during degeneration.

Collectively, our data suggest that differential distribution of the mRNAs for different actin isoforms and the corresponding actin filaments that are composed of distinct isoforms contributes to specific functions during development of motor axons by spatial regulation of actin dynamics and stability in various cellular compartments. Actα and Actγ stabilize F-actin polymers in the axon shaft and at collateral branches, thereby promoting filopodia extension, whereas Actβ provides a highly dynamic cytoskeleton in the axon, particularly in axonal growth cones, which seems to be essential for axon elongation and pathfinding. Furthermore, our data suggest that up-regulation of Actα could make a major contribution to the formation of new axonal branches and sprouting during nerve injury and in neuromuscular diseases.

Materials and methods

Enrichment of embryonic mouse motoneurons and compartmentalized culture

The isolation and enrichment of primary mouse motoneurons was performed as previously described (Wiese et al., 2010). Lumbar spinal cords were dissected from E13.5 mouse embryos, and motoneurons were enriched by panning using a p^{75NTR} antibody (Wiese et al., 1999). Isolated motoneurons were transduced with lentiviruses in suspension

and immediately plated on polyornithine- and laminin-coated plates. Cells were maintained in neurobasal medium supplied with 2% B27, 2% heat-inactivated horse serum, 500 µM Glutamax (Invitrogen), 5 ng/ml BDNF, and ciliary neurotrophic factor (CNTF) for 5 or 7 DIV in a humid CO_2 incubator. Medium was replaced 24 h after plating and then every other day. Compartmentalized microfluidic chambers were applied as described previously (Saal et al., 2014). In brief, cells were plated into one side, which served as the somatodendritic compartment. During the 7-d culture, axons grew through the microgrooves to the other compartment (the axonal compartment) as a response to a BDNF gradient, which was applied at 20 ng/ml only to the axonal compartment.

Cortical neuron culture

Cortices were dissected from E17 CD1 embryos and trypsinized (0.5%; Worthington Biochemical Corporation) for 20 min at 37°C. Cortices were washed three times with dissection medium (HBSS, 1× Na-pyruvate, 0.1% glucose, 10 mM Hepes), DNase (0.25%; Sigma-Aldrich) was added, and cortices were incubated for 5 min at RT. After two washes with dissection medium, trypsin inhibitor (0.5%; Sigma-Aldrich) was added and triturated using a Pasteur pipette. Cells were transferred into a new falcon tube, and the remaining suspension was further triturated. Cells were centrifuged at 1,400 rpm for 3 min, resuspended, and plated on poly-L-lysine coated glass coverslips or in microfluidic chambers. Cells were maintained for 5–7 d in a humid CO_2 incubator in neurobasal medium supplied with 1× B27, 0.5% penicillin/streptomycin, and 1% Glutamax.

Axonal RNA preparation and quantitative RT-PCR

Total RNA was isolated from somatodendritic and axonal compartments separately. To avoid RNA loss, RNA extraction and reverse transcription were performed in the same tube, as previously described (Durand et al., 2006). Reverse transcription buffer was prepared using 10 mM Tris/HCl, pH 8.0, 2 mM dNTP (28406557; GE Healthcare), 1 mM Random Primer N6 11034731001; Roche), 1× First Strand Buffer (18080093; Invitrogen), 10 mM DTT (18080093; Invitrogen), 0.5% NP-40 (11332473001; Roche), 20 µg glycogen (R055; Fermentas), 5 U RNasin Plus RNase Inhibitor (N2611; Promega), and RNase-free water. Cells were lysed directly in reverse transcription buffer and transferred into 0.5 ml PCR tubes. Lysates were denatured at 70°C for 2 min and immediately incubated on ice for 1 min. The tube contents were collected by a brief centrifugation and incubated at 37°C for random hexamer binding. 1 µl Superscript III Reverse transcription (18080044; Invitrogen) was added and incubated at 38°C for 2 h. Reverse transcription reaction was continued for 8 h at 39°C. As buffer components of the reverse transcription reaction might act as competitive inhibitors in subsequent PCR reactions, cDNA was purified using the QIAGEN II purification kit (20021). Isoform-specific intron-spanning primers were designed using Oligo 6.0 software (MedProbe). Primer and $MgCl_2$ concentrations were optimized for different PCR conditions. The specificity of PCR products was verified by analysis of product melting curves, DNA gel electrophoresis, minus reverse transcription, and sequencing of the corresponding amplicons. Absolute quantification was performed to determine copy numbers of each actin isoform. External calibration curves and data quantification were performed as previously described (Durand et al., 2006). In brief, PCR amplicons of each actin isoform were cloned into TOPO-TA vector. Next, cloned amplicons were cut out of the vector, purified, and quantified. Serial dilutions of 2 to 10^6 molecules were made and used as template for the quantitative RT-PCR reaction to generate external calibration curves. Y-intercept and slopes were read from calibration curves, and absolute copy numbers were determined using the following formula: copy number = $10^{(\text{cross.point} - Y)}$/slope. Absolute copy numbers of Actα, Actβ, and Actγ were normalized to absolute copy numbers of Gapdh. Gapdh was also used for data normalization of knockdown samples versus control. The purity of the axonal mRNA preparation was confirmed by the absence of Histone H1f0 transcripts in RNA fractions obtained from this compartment. 18srRNA and Gapdh were used for quality control of both somatodendritic and axonal RNA preparations.

The following primers were used for quantitative RT-PCR: Actα, 5′-TAGACACCATGTGCGACGAAGA-3′ (forward), 5′-ACCTAC CATGACACCCTGGTGA-3′ (reverse); Actβ, 5′-GATGACCCAGAT CATGTTT-3′ (forward), 5′-CGTGAGGGAGAGCATAG-3′ (reverse); Actγ, 5′-ATCGCCGCACTCGTCAT-3′ (forward), 5′-GCCGTGTTC GATAGGGTA-3′ (reverse); Gapdh, 5′-AACTCCCACTCTTCCACC TTC-3′ (forward), 5′-GGTCCAGGGTTTCTTACTCCTT-3′ (reverse); and histone H1f0, 5′-CCCAAGTATTCAGACATGAT-3′ (forward), 5′-CGCTTGATGGACAACT-3′ (reverse).

Laser capture microdissection

Laser capture microdissection was performed as previously described (See et al., 2014). In brief, lumbar spinal cords of E18 embryos and 12-wk-old mice were dissected and embedded in optimum cutting temperature compound (Tissue-Tek), dipped shortly in isopentane, and immediately frozen in liquid nitrogen. 15-µm cross sections were prepared using a cryostat (Leica Biosystems), transferred to 0.9-µm polyester membranes, and stained in Cresyl Violet solution. Somata of motoneurons were cut from ventral horn of the spinal cord using a DM6000B laser microdissection system (Leica Biosystems) equipped with a 20× 0.4-NA objective and lysed in reverse transcription buffer. cDNA was made from total RNA using Superscript III and subsequently analyzed by quantitative RT-PCR as described in the previous paragraph.

Cloning and lentivirus production

Myristoylated and palmitoylated eGFP ($eGFP^{myr}$) reporters were used to investigate the local translation of actin mRNAs in axon shafts and axon terminals of primary motoneurons (Rathod et al., 2012). 3′ UTRs of Actα, Actβ, and Actγ mRNAs were inserted into an $eGFP^{myr}$ expression cassette using an FU-based lentiviral vector (Fig. 3 A). Specific shRNA oligonucleotides targeted against the 3′ UTRs of individual actin isoforms were designed and cloned into pSIH-H1 shRNA vector (System Bioscience) according to the manufacturer's instructions. GFP was used as a marker to identify transduced cells. A luciferase pSIH-H1 vector was used as a control. The following antisense sequences were used for shRNA cloning: Actα-construct 1, 5′-CAG GACGACAATCGACAAT-3′; Actα-construct 2, 5′-CAATCGACA ATCGTGCTGT-3′; Actβ-construct 1, 5′-GCACACCTTACCTTA CACA-3′; Actβ-construct 2, 5′-GTGCACACCTTACCTTACA-3′; Actγ-construct-1, 5′-GCACGCTGTAGATGAGAAA-3′; Actγ-construct 2: 5′-GCACGATGAAGATTAAGAT-3; and Actγ-construct 3, 5′-CTAGCACGATGAAGATTAA-3′.

For expression vectors of actin isoforms, plasmids containing coding sequence and 3′ UTR of mouse Actα, Actβ, and Actγ were purchased from Harvard plasmid database and subcloned into an FU-based lentiviral vector containing an HA tag at the N terminus. For generation of Actβ rescue construct, the coding sequence and 3′ UTR of mouse Actβ were amplified by PCR using HA-tagged Actβ vector as the template. To make the rescue construct resistant to shRNA, the sequence within 3′ UTR of Actβ mRNA which is targeted by the shRNA was deleted. This sequence is located directly 3′ after the poly(A) site and is not involved in binding of known RNA-binding proteins. The PCR product was inserted into an expression vector containing ubiquitin promotor. The ubiquitin-Actβ-rescue cassette was then excised and cloned into pSIH-H1 vector containing shActβ.

Lentiviral particles were packaged in HEK^{293T} cells with pCMV-VSVG and pCMVΔR8.91 helper plasmids as described previously (Rehberg et al., 2008). Cells were transfected with Lipofectamine 2000 (Invitrogen) in OptiMEM medium with 10% fetal calf serum for 12–14 h, and viral supernatants were harvested 72 h after transfection by ultracentrifugation. Virus titer was tested in NSC34 cells.

G- to F-actin separation and Western blotting

Approximately 300,000 primary motoneurons were plated on polyornithine- and laminin-coated 24-well cell culture dishes for 7 DIV. Cells were washed two times with prewarmed PBS and lysed by directly adding 2× Laemmli buffer (125 mM Tris, pH 6.8, 10% SDS, 50% glycerol, 25% β-mercaptoethanol, and 0.2% bromophenol blue). Protein lysates were boiled at 99°C for 5 min and centrifuged briefly at 4°C. Protein extracts were separated on SDS-PAGE gels and blotted onto nitrocellulose membranes. For G- and F-actin separation, cells were homogenized in actin stabilization buffer containing 0.1 M Pipes, pH 6.9, 30% glycerol (vol/vol), 5% DMSO (vol/vol), 1 mM $MgSO_4$, 1 mM EGTA, 1% Triton X-100 (vol/vol), 1 mM ATP, complete protease inhibitor, and phosphatase inhibitor for 10 min at 37°C. Protein extracts were collected in a tube and centrifuged at 100,000 *g* in an ultracentrifuge (Beckman TLA 12.2) for 75 min at 37°C. Supernatants containing G-actin were recovered, and pellets containing F-actin were collected separately. Pellets were resuspended in RIPA buffer, and total protein concentration was quantified using a BCA protein assay kit (Thermo Fisher Scientific). Equal amounts of proteins were loaded for both G- and F-actin fractions. Membranes were probed with the following primary antibodies overnight: mouse monoclonal anti-Smn (1:4,000, 610646; BD), mouse monoclonal anti–pan actin (1:3,000, MAB1501R; EMD Millipore), goat polyclonal anti-Calnexin (1:5,000, AB0037-200; Acris), rat monoclonal anti-HA (1:5,000, 11867423001; Roche), mouse monoclonal anti-Actα (5C5.F8.C7; Crawford et al., 2002; 1:2,500, MA5-12542; Thermo Fisher Scientific), mouse monoclonal anti-Actβ (1:4,000, GTX26276; GeneTex), mouse monoclonal anti-Actγ (2–4; Schreiber et al., 2015; 1:8,000, sc-65634; Santa Cruz Biotechnology, Inc.), mouse monoclonal anti-Gapdh (1:5,000, CB1001; EMD Millipore), and secondary antibodies: goat anti-mouse IgG (1:10,000, 115–035-003; Jackson ImmunoResearch Laboratories, Inc.), donkey anti–goat IgG (1:10,000, 705–545-147; Jackson ImmunoResearch Laboratories, Inc.), and goat anti-rat IgG (1:10,000, 112–035-003; Jackson ImmunoResearch Laboratories, Inc.) for 1 h at RT and developed using ECL systems (GE Healthcare).

High-resolution in situ hybridization and data analysis

High-resolution in situ hybridization was performed following the manufacturer's instructions (Panomics) with minor modifications. In brief, cells were fixed with paraformaldehyde lysine phosphate (PLP) buffer, pH 7.4, containing 4% PFA, 5.4% glucose, and 0.01 M sodium metaperiodate for 10 min at RT and washed with RNase-free PBS. Cells were permeabilized using a supplied detergent solution (Panomics) for 4 min at RT. To unmask mRNAs from bound proteins, proteinase K was added at 1:8,000 dilution and incubated for 4 min. Next, isoform specific hybridization probes were diluted 1:100 in hybridization buffer and incubated at 40°C overnight. In triplex assays, all three specific probes detecting Actα, Actβ, and Actγ were added to the hybridization buffer, and cells were incubated with this mixture. Three independent signal amplification systems allowed fluorescent detection of all three actin isoforms in a single experiment. Preamplifier, amplifier, and label probe oligonucleotides were diluted 1:25 in corresponding buffers and incubated each for 1 h at 40°C, respectively. Cells were then washed three times with supplied wash buffer (Panomics) at RT. To visualize axons, Tau immunostaining was performed (see immunofluorescence section for details). Antisense probes against mouse Actα, Actβ, Actγ, Gapdh, 18srRNA, and *Escherichia coli*–DapB transcripts were designed by and obtained from Panomics. For in situ hybridization with an LNA probe, cells were fixed with PLP buffer at RT for 15 min and then permeabilized in 0.3% Triton X-100 for 5 min. Prehybridization solution containing 10% formamide, 10% dextran sulfate, 1× Denhart's, 0.5 mg/ml salmon sperm DNA, 0.5 mg/ml *E. coli* tRNA, and 0.05 M EDTA in 4× SSC was added onto coverslips and incubated at 37°C for 1 h. 35 nM digoxigenin (DIG)–labeled antisense Actα LNA probe was diluted in hybridization buffer, denatured at 80°C for 75 s, and hybridized at 37°C overnight. Coverslips were washed three times for 10 min each with 1× SSC/0.1% Tween-20 at 37°C followed by three 1-min washes with 0.1× SSC/0.1% Tween-20 at RT. For immunofluorescence detection of DIG-labeled Actα probe, cells were blocked with 15% goat serum, 2% BSA, and 5% sucrose for 1 h at RT. Primary (mouse anti-DIG) and secondary antibodies were incubated at RT for 1 h and washed three times for 10 min each with PBS containing 0.1% Triton X-100. The probe sequence was 5′-AGT CAATCTATGTACACGTCAA-3′. 12-bit images were acquired with an Olympus Fluoview 1000 confocal system equipped with a 60× 1.35-NA oil objective, at 1,024 × 1,024-pixel resolution. Maximum intensity projections were created of 4-µm z-stacks.

Live-cell extraction and immunofluorescence

For immunofluorescence detection, motoneurons were cultured on laminin and polyornithine-coated glass coverslips for 5 or 7 DIV. Cells were washed two times with prewarmed PBS and fixed with 4% PLP buffer at RT for 15 min. For Actα immunostaining, cells were permeabilized with 0.1% Triton X-100 at RT for 15 min. For Actβ and Actγ staining, cells were first exposed to ice-cold methanol for 5 min at −20°C and permeabilized with 0.3% Triton X-100 at RT for 10 min. For DBP staining, cells were exposed to ice-cold acetone for 5 min at −20°C. For all other antibodies, cells were permeabilized with 0.3% Triton X-100 at RT for 20 min. After three washes in PBS, blocking solution containing 15% goat or donkey serum, 2% BSA, and 5% sucrose in PBS was added onto coverslips and incubated at RT for 1 h. Actα antibody was incubated in blocking solution at RT for 3 h. Other primary antibodies were incubated in blocking solution at 4°C overnight. Secondary antibodies were added for 1 h at RT, and nuclei were counterstained with DAPI. Alexa Fluor 546 phalloidin (A22283; Invitrogen) was added at 1:50 in PBS after incubation with secondary antibodies. Coverslips were washed and mounted using Aqua Poly/Mount (18606; Polysciences) and subsequently imaged. For live-cell extraction, cultured neurons were extracted either with 0.01% saponin for 10 s or 0.25% Triton X-100 and 0.3% glutaraldehyde for 1 min in a cytoskeleton buffer (10 mM MES, pH 6.1, 150 mM NaCl, 5 mM EGTA, 5 mM glucose and 5 mM $MgCl_2$) to maintain the actin ultrastructure (Auinger and Small, 2008; Lee et al., 2013). After saponin extraction, cells were washed briefly and fixed with 4% PLP. After Triton X-100 extraction, samples were postfixed for 15 min in 2% glutaraldehyde in cytoskeleton buffer. Samples were incubated with block solution for 1 h at RT, and primary and secondary antibodies were applied as described above.

5 µg/ml DBP (345802; EMD Millipore) was used for labeling of G-actin (Van Baelen et al., 1980; Lee et al., 2013). Other primary and secondary antibodies used were polyclonal rabbit anti-Tau (1:1,000, T6402; Sigma-Aldrich), monoclonal mouse anti–α-Tubulin (1:1,000, T5168; Sigma-Aldrich), monoclonal mouse anti-Map2 (1:1,000, M1406; Sigma-Aldrich), monoclonal mouse anti-Actα (5C5.F8.C7; 1:500, MA5-12542; Thermo Fisher Scientific), monoclonal mouse anti-Actβ (1:1,000, GTX26276; GeneTex), monoclonal mouse anti-Actγ (2–4; 1:1,000, sc-65634; Santa Cruz Biotechnology, Inc.), monoclonal mouse anti-DIG (21H8; 1:500, ab420; Abcam), monoclonal rat anti-HA

(1:1,000, 1186742300; Roche), polyclonal rabbit anti-DBP (5 µg/ml, PA5-19802; Thermo Fisher Scientific), monoclonal mouse anti-Gapdh (1:1,000, CB1001; EMD Millipore), goat anti–rabbit IgG (H+L; DyLight 405, 1:250, 111334; Jackson ImmunoResearch Laboratories, Inc.), donkey anti-rabbit (H+L; Cy3, 1:400, 711-165-152; Jackson ImmunoResearch Laboratories, Inc.), goat anti-rabbit (H+L; Cy5, 1:400, A21070; Invitrogen), donkey anti–rat IgG (H+L; Cy3, 1:500, 712-165-150; Jackson ImmunoResearch Laboratories, Inc.), goat anti–mouse IgG (H+L; Cy3, 1:500, 115-165-146; Jackson ImmunoResearch Laboratories, Inc.), goat anti–mouse IgG (H+L; Cy5, 1:500, 115-175-146; Jackson ImmunoResearch Laboratories, Inc.), goat anti–mouse IgM (DyLight 550, 1:500, SA5-10151; Thermo Fisher Scientific), goat anti–mouse IgM (Alexa Fluor 488, 1:500, A-21042; Thermo Fisher Scientific), goat anti–mouse IgG1 (Alexa Fluor 488, 1:500; A21121; Thermo Fisher Scientific).

Image acquisition and analysis of neurite growth

For viability assays, cells were plated on laminin- and polyornithine-coated plastic surface in a four-well dish (627170; Greiner bio-one) and counted 18 h after plating and again at DIV7. For growth cone size analysis, cells were plated on a neuromuscular synapse specific laminin isoform (laminin 221) for 5 d and stained against Tau and phalloidin. For soma size, length, and number of dendrites, images were acquired with an Olympus Fluoview 1000 confocal system using a 60× 1.35-NA oil objective. Single or multiple 12-bit image stacks were taken with 800 × 800–pixel resolution. For axon length and branching analysis images were acquired with a Keyence BZ-8000K fluorescence microscope equipped with a standard color camera using a 20× 0.7-NA objective.

Images were processed using ImageJ 1.42I software (Schneider et al., 2012). For better visibility, linear contrast enhancement was applied to Figs. 2–8, 10, S1, S2, S4, and S5 using Adobe Photoshop 7.0, and the same stetting was used for both knockdown and control groups. For all statistical analyses GraphPad Prism 5.02 software was used. Data are depicted in box and whisker plots unless otherwise indicated. The line inside the box indicates the median, and a plus sign indicates the mean value. Boxes represent 10–90% of the data, and outliers are plotted as individual dots.

FRAP

Primary motoneurons were transduced with isoform-specific eGFP-^{myr}-reporter constructs and cultured on µ-dishes (Ibidi) for 5 DIV in presence of 10 ng/µl BDNF and CNTF. Fluorescence recovery after photobleaching was measured as previously described with few modifications in data analysis (Rathod et al., 2012). FRAP experiments were performed with an inverted SP5 confocal microscope (Leica Biosystems) using a 60× 1.35-NA oil objective. 8-bit images were taken with 512 × 512 pixel resolution. Prior to bleaching, eight images were taken at 30-s intervals using 19% laser intensity. A 100-µm segment of the distal axon was bleached for 50 frames using 80% laser power (Leica Biosystems 488-nm laser line) at ∼3 Hz speed. Recovery was monitored for 1 h after bleach at 30-s intervals. The after-bleach recovery was calculated as the mean intensity of gray values per pixel in defined regions of interest of axonal branch points and axonal growth cones after background subtraction using LAS lite software (Leica Biosystems). F0 was defined as the mean of mean intensities from eight prebleach images. The mean of signal intensities of 10 immediate after bleach images was subtracted from measured after bleach signal intensities to eliminate the remaining signal immediately after bleaching. These values were then normalized to F0 to calculate the percentage recovery. In control experiments, cells were treated with protein synthesis inhibitors (50 ng/ml anisomycin for 2 h before imaging or 10 µg/ml cycloheximide overnight before the FRAP experiment).

Live-cell imaging and data quantification

Live-cell imaging was performed with an inverted epifluorescence microscope (TE2000; Nikon) equipped with 60× 1.4-NA objective and heated stage chamber (TOKAI HIT CO., LTD) at 37°C and 5% CO_2. Motoneurons were transduced with lentiviral constructs coexpressing GFP and shRNAs directed against individual actin isoforms and cultured on µ-dishes (Ibidi) for 6 DIV. Immediately before imaging, medium was replaced with neurobasal medium without phenol red supplied with 2% B27, 2% horse serum, and 10 ng/ml BDNF and CNTF. Cells were then taken to the microscope and maintained constantly at 37°C on a heated stage chamber. GFP was excited using a 470-nm cool LED PE-100 light source at 2–4% light emission intensity. Dynamics of growth cone filopodia or axonal filopodia were monitored for 40 min at 20-s intervals by time-lapse imaging. 12-bit images of 1,024 × 1,024 pixels were acquired with an Orca Flash 4.0 V2 camera (Hamamatsu Photonics), controlled by Nikon Element image software (Nikon). For quantification of the axonal filopodia dynamics, (1) frequency of filopodia initiation, (2) filopodia life time, (3) rate of filopodia dynamic movement, and (4) total absolute changes in length for individual filopodia were analyzed. For the rate of filopodia dynamics, only filopodia extensions or retractions with a minimum length of 1 µm were included. The number of dynamic movements was determined for each single filopodium, and the mean frequency of 50 filopodia was represented in a box and whisker graph. To determine the total change in filopodia length, the length of individual filopodia was measured in all 120 frames. The total change in length was calculated by summing absolute length changes between subsequent frames that showed a change of at least 1 µm. The mean total changes in length of 50 filopodia were displayed in a box and whisker plot. For quantification of filopodia dynamics in growth cones, maximum projection of all 120 frames was used for generating a multiple kymograph using an ImageJ plug-in. To obtain the central point of the growth cone, all 120 frames were first staked into a Z-projection image. The central point obtained from the stack image was selected and copied back into the time-lapse movie. Using an ImageJ plugin, a multiple kymograph was created with time on the x axis and distance on the y axis. To calculate the mean speed of growth cone movement, the length of each pick (20 s) was measured from the x axis and y axis. The velocity of filopodia/lamellipodia movement was measured as delta length in micrometers divided by the time in seconds for each pick (Sivadasan et al., 2016).

Online supplemental material

Fig. S1 shows high-resolution in situ hybridization. Fig. S2 shows validation of Actα-, Actβ-, and Actγ-specific antibodies by Western blot and immunocytochemistry experiments. Fig. S3 shows that shRNA knockdown of actin isoforms generates distinct phenotypes that are result of actin isoform–specific depletion and not off-target effects. Fig. S4 shows that reexpression of Actβ rescues axon elongation and growth cone formation defects in Actβ-depleted motoneurons. Fig. S5 shows expression of actin isoforms in primary cortical neurons. Video 1 shows axonal filopodia dynamics in cultured motoneurons. Video 2 shows that depletion of Actα disturbs growth dynamics of axonal filopodia. Video 3 shows that depletion of Actβ does not affect growth dynamics of axonal filopodia. Video 4 shows that depletion of Actγ reduces growth dynamics of axonal filopodia. Video 5 shows that axonal growth cones show highly dynamic filopodia activity. Video 6 shows that knockdown of Actα does not disturb axonal growth cone filopodia movements. Video 7 shows that dynamic movements of axonal growth cone filopodia are reduced in Actβ knockdown motoneurons. Video 8 shows that Actγ depletion does not impair axonal growth cone filopodia dynamics.

Acknowledgments

We thank Regine Sendtner for help with animal breeding, Hildegard Troll and Elke Spirk for help with virus production, Dr. Sibylle Jablonka for help and suggestions in preparation of figures, Michaela Kessler and Hanaa Ghanawi for help with primary cultures, and Anna Maria Musti for helpful and interesting discussions.

M. Moradi was supported by a grant from the Deutsche Forschungsgemeinschaft project SPP 1738 and project SE697/5-1 and the Hermann-and-Lilli Schilling Stiftung. The project was further supported by the Bavarian excellence program ForIPS (D2-F2412,26), Bundesministerium für Bildung und Forschung Dystract TP6, and the European Community's Health Seventh Framework Programme (FP7/2007-2013) under grant agreement number 259867 (EUROMOTOR).

The authors declare no competing financial interests.

Author contributions: M. Sendtner and M. Moradi designed the experiments and wrote the manuscript. R. Sivadasan, L. Saal, P. Lüningschrör, B. Dombert, and R.J. Rathod contributed to the experiments. R. Blum and D.C. Dieterich gave technical support.

Submitted: 27 April 2016
Revised: 11 November 2016
Accepted: 17 January 2017

References

Allen, P.G., C.B. Shuster, J. Käs, C. Chaponnier, P.A. Janmey, and I.M. Herman. 1996. Phalloidin binding and rheological differences among actin isoforms. *Biochemistry.* 35:14062–14069. http://dx.doi.org/10.1021/bi961326g

Andersen, P.M., and A. Al-Chalabi. 2011. Clinical genetics of amyotrophic lateral sclerosis: What do we really know? *Nat. Rev. Neurol.* 7:603–615. http://dx.doi.org/10.1038/nrneurol.2011.150

Auinger, S., and J.V. Small. 2008. Correlated light and electron microscopy of the cytoskeleton. *Methods Cell Biol.* 88:257–272. http://dx.doi.org/10.1016/S0091-679X(08)00414-7

Baciu, C., K.J. Thompson, J.L. Mougeot, B.R. Brooks, and J.W. Weller. 2012. The LO-BaFL method and ALS microarray expression analysis. *BMC Bioinformatics.* 13:244. http://dx.doi.org/10.1186/1471-2105-13-244

Bareyre, F.M., B. Haudenschild, and M.E. Schwab. 2002. Long-lasting sprouting and gene expression changes induced by the monoclonal antibody IN-1 in the adult spinal cord. *J. Neurosci.* 22:7097–7110.

Bassell, G.J., H. Zhang, A.L. Byrd, A.M. Femino, R.H. Singer, K.L. Taneja, L.M. Lifshitz, I.M. Herman, and K.S. Kosik. 1998. Sorting of β-actin mRNA and protein to neurites and growth cones in culture. *J. Neurosci.* 18:251–265.

Belyantseva, I.A., B.J. Perrin, K.J. Sonnemann, M. Zhu, R. Stepanyan, J. McGee, G.I. Frolenkov, E.J. Walsh, K.H. Friderici, T.B. Friedman, and J.M. Ervasti. 2009. Gamma-actin is required for cytoskeletal maintenance but not development. *Proc. Natl. Acad. Sci. USA.* 106:9703–9708. http://dx.doi.org/10.1073/pnas.0900221106

Bergeron, S.E., M. Zhu, S.M. Thiem, K.H. Friderici, and P.A. Rubenstein. 2010. Ion-dependent polymerization differences between mammalian β- and γ-nonmuscle actin isoforms. *J. Biol. Chem.* 285:16087–16095. http://dx.doi.org/10.1074/jbc.M110.110130

Blöchlinger, S., O. Weinmann, M.E. Schwab, and M. Thallmair. 2001. Neuronal plasticity and formation of new synaptic contacts follow pyramidal lesions and neutralization of Nogo-A: A light and electron microscopic study in the pontine nuclei of adult rats. *J. Comp. Neurol.* 433:426–436. http://dx.doi.org/10.1002/cne.1150

Bosch-Marcé, M., C.D. Wee, T.L. Martinez, C.E. Lipkes, D.W. Choe, L. Kong, J.P. Van Meerbeke, A. Musarò, and C.J. Sumner. 2011. Increased IGF-1 in muscle modulates the phenotype of severe SMA mice. *Hum. Mol. Genet.* 20:1844–1853. http://dx.doi.org/10.1093/hmg/ddr067

Buckmaster, P.S., and X. Wen. 2011. Rapamycin suppresses axon sprouting by somatostatin interneurons in a mouse model of temporal lobe epilepsy. *Epilepsia.* 52:2057–2064. http://dx.doi.org/10.1111/j.1528-1167.2011.03253.x

Bunnell, T.M., and J.M. Ervasti. 2010. Delayed embryonic development and impaired cell growth and survival in Actg1 null mice. *Cytoskeleton.* 67:564–572. http://dx.doi.org/10.1002/cm.20467

Bunnell, T.M., B.J. Burbach, Y. Shimizu, and J.M. Ervasti. 2011. β-Actin specifically controls cell growth, migration, and the G-actin pool. *Mol. Biol. Cell.* 22:4047–4058. http://dx.doi.org/10.1091/mbc.E11-06-0582

Cajigas, I.J., G. Tushev, T.J. Will, S. tom Dieck, N. Fuerst, and E.M. Schuman. 2012. The local transcriptome in the synaptic neuropil revealed by deep sequencing and high-resolution imaging. *Neuron.* 74:453–466. http://dx.doi.org/10.1016/j.neuron.2012.02.036

Campbell, D.S., and C.E. Holt. 2001. Chemotropic responses of retinal growth cones mediated by rapid local protein synthesis and degradation. *Neuron.* 32:1013–1026. http://dx.doi.org/10.1016/S0896-6273(01)00551-7

Cheever, T.R., E.A. Olson, and J.M. Ervasti. 2011. Axonal regeneration and neuronal function are preserved in motor neurons lacking β-actin in vivo. *PLoS One.* 6:e17768. http://dx.doi.org/10.1371/journal.pone.0017768

Cheever, T.R., B. Li, and J.M. Ervasti. 2012. Restricted morphological and behavioral abnormalities following ablation of β-actin in the brain. *PLoS One.* 7:e32970. http://dx.doi.org/10.1371/journal.pone.0032970

Chen, M.S., A.B. Huber, M.E. van der Haar, M. Frank, L. Schnell, A.A. Spillmann, F. Christ, and M.E. Schwab. 2000. Nogo-A is a myelin-associated neurite outgrowth inhibitor and an antigen for monoclonal antibody IN-1. *Nature.* 403:434–439. http://dx.doi.org/10.1038/35000219

Chia, P.H., B. Chen, P. Li, M.K. Rosen, and K. Shen. 2014. Local F-actin network links synapse formation and axon branching. *Cell.* 156:208–220. http://dx.doi.org/10.1016/j.cell.2013.12.009

Cifuentes-Diaz, C., S. Nicole, M.E. Velasco, C. Borra-Cebrian, C. Panozzo, T. Frugier, G. Millet, N. Roblot, V. Joshi, and J. Melki. 2002. Neurofilament accumulation at the motor endplate and lack of axonal sprouting in a spinal muscular atrophy mouse model. *Hum. Mol. Genet.* 11:1439–1447. http://dx.doi.org/10.1093/hmg/11.12.1439

Crawford, T.O., and C.A. Pardo. 1996. The neurobiology of childhood spinal muscular atrophy. *Neurobiol. Dis.* 3:97–110. http://dx.doi.org/10.1006/nbdi.1996.0010

Crawford, K., R. Flick, L. Close, D. Shelly, R. Paul, K. Bove, A. Kumar, and J. Lessard. 2002. Mice lacking skeletal muscle actin show reduced muscle strength and growth deficits and die during the neonatal period. *Mol. Cell. Biol.* 22:5887–5896. http://dx.doi.org/10.1128/MCB.22.16.5887-5896.2002

De La Cruz, E.M. 2005. Cofilin binding to muscle and non-muscle actin filaments: Isoform-dependent cooperative interactions. *J. Mol. Biol.* 346:557–564. http://dx.doi.org/10.1016/j.jmb.2004.11.065

Dent, E.W., and K. Kalil. 2001. Axon branching requires interactions between dynamic microtubules and actin filaments. *J. Neurosci.* 21:9757–9769.

Donnelly, C.J., D.E. Willis, M. Xu, C. Tep, C. Jiang, S. Yoo, N.C. Schanen, C.B. Kirn-Safran, J. van Minnen, A. English, et al. 2011. Limited availability of ZBP1 restricts axonal mRNA localization and nerve regeneration capacity. *EMBO J.* 30:4665–4677. http://dx.doi.org/10.1038/emboj.2011.347

Donnelly, C.J., M. Park, M. Spillane, S. Yoo, A. Pacheco, C. Gomes, D. Vuppalanchi, M. McDonald, H.H. Kim, T.T. Merianda, et al. 2013. Axonally synthesized β-actin and GAP-43 proteins support distinct modes of axonal growth. *J. Neurosci.* 33:3311–3322. http://dx.doi.org/10.1523/JNEUROSCI.1722-12.2013

Dugina, V., I. Zwaenepoel, G. Gabbiani, S. Clément, and C. Chaponnier. 2009. Beta and gamma-cytoplasmic actins display distinct distribution and functional diversity. *J. Cell Sci.* 122:2980–2988. http://dx.doi.org/10.1242/jcs.041970

Durand, G.M., N. Marandi, S.D. Herberger, R. Blum, and A. Konnerth. 2006. Quantitative single-cell RT-PCR and Ca^{2+} imaging in brain slices. *Pflugers Arch.* 451:716–726. http://dx.doi.org/10.1007/s00424-005-1514-3

Dwivedy, A., F.B. Gertler, J. Miller, C.E. Holt, and C. Lebrand. 2007. Ena/VASP function in retinal axons is required for terminal arborization but not pathway navigation. *Development.* 134:2137–2146. http://dx.doi.org/10.1242/dev.002345

Ferraiuolo, L., J. Kirby, A.J. Grierson, M. Sendtner, and P.J. Shaw. 2011. Molecular pathways of motor neuron injury in amyotrophic lateral sclerosis. *Nat. Rev. Neurol.* 7:616–630. http://dx.doi.org/10.1038/nrneurol.2011.152

Gallo, G. 2011. The cytoskeletal and signaling mechanisms of axon collateral branching. *Dev. Neurobiol.* 71:201–220. http://dx.doi.org/10.1002/dneu.20852

Gordon, T., and N. Tyreman. 2010. Sprouting capacity of lumbar motoneurons in normal and hemisected spinal cords of the rat. *J. Physiol.* 588:2745–2768. http://dx.doi.org/10.1113/jphysiol.2010.190389

Hirokawa, N., K. Sobue, K. Kanda, A. Harada, and H. Yorifuji. 1989. The cytoskeletal architecture of the presynaptic terminal and molecular structure of synapsin 1. *J. Cell Biol.* 108:111–126. http://dx.doi.org/10.1083/jcb.108.1.111

Jablonka, S., M. Beck, B.D. Lechner, C. Mayer, and M. Sendtner. 2007. Defective Ca^{2+} channel clustering in axon terminals disturbs excitability in motoneurons in spinal muscular atrophy. *J. Cell Biol.* 179:139–149. http://dx.doi.org/10.1083/jcb.200703187

Jaeger, M.A., K.J. Sonnemann, D.P. Fitzsimons, K.W. Prins, and J.M. Ervasti. 2009. Context-dependent functional substitution of α-skeletal actin by γ-cytoplasmic actin. *FASEB J.* 23:2205–2214. http://dx.doi.org/10.1096/fj.09-129783

Kalil, K., and E.W. Dent. 2014. Branch management: mechanisms of axon branching in the developing vertebrate CNS. *Nat. Rev. Neurosci.* 15:7–18. http://dx.doi.org/10.1038/nrn3650

Kariya, S., G.H. Park, Y. Maeno-Hikichi, O. Leykekhman, C. Lutz, M.S. Arkovitz, L.T. Landmesser, and U.R. Monani. 2008. Reduced SMN protein impairs maturation of the neuromuscular junctions in mouse models of spinal muscular atrophy. *Hum. Mol. Genet.* 17:2552–2569. http://dx.doi.org/10.1093/hmg/ddn156

Kislauskis, E.H., Z. Li, R.H. Singer, and K.L. Taneja. 1993. Isoform-specific 3′-untranslated sequences sort α-cardiac and β-cytoplasmic actin messenger RNAs to different cytoplasmic compartments. *J. Cell Biol.* 123:165–172. http://dx.doi.org/10.1083/jcb.123.1.165

Kong, L., X. Wang, D.W. Choe, M. Polley, B.G. Burnett, M. Bosch-Marcé, J.W. Griffin, M.M. Rich, and C.J. Sumner. 2009. Impaired synaptic vesicle release and immaturity of neuromuscular junctions in spinal muscular atrophy mice. *J. Neurosci.* 29:842–851. http://dx.doi.org/10.1523/JNEUROSCI.4434-08.2009

Kumar, A., K. Crawford, L. Close, M. Madison, J. Lorenz, T. Doetschman, S. Pawlowski, J. Duffy, J. Neumann, J. Robbins, et al. 1997. Rescue of cardiac α-actin-deficient mice by enteric smooth muscle γ-actin. *Proc. Natl. Acad. Sci. USA.* 94:4406–4411. http://dx.doi.org/10.1073/pnas.94.9.4406

Kumar, A., K. Crawford, R. Flick, R. Klevitsky, J.N. Lorenz, K.E. Bove, J. Robbins, and J.L. Lessard. 2004. Transgenic overexpression of cardiac actin in the mouse heart suggests coregulation of cardiac, skeletal and vascular actin expression. *Transgenic Res.* 13:531–540. http://dx.doi.org/10.1007/s11248-004-2823-6

Larsson, H., and U. Lindberg. 1988. The effect of divalent cations on the interaction between calf spleen profilin and different actins. *Biochim. Biophys. Acta.* 953:95–105. http://dx.doi.org/10.1016/0167-4838(88)90013-1

Lee, C.W., E.A. Vitriol, S. Shim, A.L. Wise, R.P. Velayutham, and J.Q. Zheng. 2013. Dynamic localization of G-actin during membrane protrusion in neuronal motility. *Curr. Biol.* 23:1046–1056. http://dx.doi.org/10.1016/j.cub.2013.04.057

Letourneau, P.C. 2009. Actin in axons: Stable scaffolds and dynamic filaments. *Results Probl. Cell Differ.* 48:65–90. http://dx.doi.org/10.1007/400_2009_15

Leung, K.M., F.P. van Horck, A.C. Lin, R. Allison, N. Standart, and C.E. Holt. 2006. Asymmetrical β-actin mRNA translation in growth cones mediates attractive turning to netrin-1. *Nat. Neurosci.* 9:1247–1256. http://dx.doi.org/10.1038/nn1775

Ling, K.K., R.M. Gibbs, Z. Feng, and C.P. Ko. 2012. Severe neuromuscular denervation of clinically relevant muscles in a mouse model of spinal muscular atrophy. *Hum. Mol. Genet.* 21:185–195. http://dx.doi.org/10.1093/hmg/ddr453

Luo, L. 2002. Actin cytoskeleton regulation in neuronal morphogenesis and structural plasticity. *Annu. Rev. Cell Dev. Biol.* 18:601–635. http://dx.doi.org/10.1146/annurev.cellbio.18.031802.150501

McWhorter, M.L., U.R. Monani, A.H. Burghes, and C.E. Beattie. 2003. Knockdown of the survival motor neuron (Smn) protein in zebrafish causes defects in motor axon outgrowth and pathfinding. *J. Cell Biol.* 162:919–931. http://dx.doi.org/10.1083/jcb.200303168

Micheva, K.D., A. Vallée, C. Beaulieu, I.M. Herman, and N. Leclerc. 1998. β-Actin is confined to structures having high capacity of remodelling in developing and adult rat cerebellum. *Eur. J. Neurosci.* 10:3785–3798. http://dx.doi.org/10.1046/j.1460-9568.1998.00391.x

Minis, A., D. Dahary, O. Manor, D. Leshkowitz, Y. Pilpel, and A. Yaron. 2014. Subcellular transcriptomics-dissection of the mRNA composition in the axonal compartment of sensory neurons. *Dev. Neurobiol.* 74:365–381. http://dx.doi.org/10.1002/dneu.22140

Murray, L.M., L.H. Comley, D. Thomson, N. Parkinson, K. Talbot, and T.H. Gillingwater. 2008. Selective vulnerability of motor neurons and dissociation of pre- and post-synaptic pathology at the neuromuscular junction in mouse models of spinal muscular atrophy. *Hum. Mol. Genet.* 17:949–962. http://dx.doi.org/10.1093/hmg/ddm367

Ning, K., C. Drepper, C.F. Valori, M. Ahsan, M. Wyles, A. Higginbottom, T. Herrmann, P. Shaw, M. Azzouz, and M. Sendtner. 2010. PTEN depletion rescues axonal growth defect and improves survival in SMN-deficient motor neurons. *Hum. Mol. Genet.* 19:3159–3168. http://dx.doi.org/10.1093/hmg/ddq226

Nowak, K.J., D. Wattanasirichaigoon, H.H. Goebel, M. Wilce, K. Pelin, K. Donner, R.L. Jacob, C. Hübner, K. Oexle, J.R. Anderson, et al. 1999. Mutations in the skeletal muscle alpha-actin gene in patients with actin myopathy and nemaline myopathy. *Nat. Genet.* 23:208–212. http://dx.doi.org/10.1038/13837

Nowak, K.J., G. Ravenscroft, C. Jackaman, A. Filipovska, S.M. Davies, E.M. Lim, S.E. Squire, A.C. Potter, E. Baker, S. Clément, et al. 2009. Rescue of skeletal muscle α-actin-null mice by cardiac (fetal) α-actin. *J. Cell Biol.* 185:903–915. http://dx.doi.org/10.1083/jcb.200812132

Nyman, T., H. Schüler, E. Korenbaum, C.E. Schutt, R. Karlsson, and U. Lindberg. 2002. The role of MeH73 in actin polymerization and ATP hydrolysis. *J. Mol. Biol.* 317:577–589. http://dx.doi.org/10.1006/jmbi.2002.5436

Ohlsson, M., H. Tajsharghi, N. Darin, M. Kyllerman, and A. Oldfors. 2004. Follow-up of nemaline myopathy in two patients with novel mutations in the skeletal muscle α-actin gene (ACTA1). *Neuromuscul. Disord.* 14:471–475. http://dx.doi.org/10.1016/j.nmd.2004.05.016

Perrin, B.J., and J.M. Ervasti. 2010. The actin gene family: Function follows isoform. *Cytoskeleton.* 67:630–634. http://dx.doi.org/10.1002/cm.20475

Porter, B.E., J. Weis, and J.R. Sanes. 1995. A motoneuron-selective stop signal in the synaptic protein S-laminin. *Neuron.* 14:549–559. http://dx.doi.org/10.1016/0896-6273(95)90311-9

Qiu, L.F., T.J. Lu, X.L. Hu, Y.H. Yi, W.P. Liao, and Z.Q. Xiong. 2009. Limbic epileptogenesis in a mouse model of fragile X syndrome. *Cereb. Cortex.* 19:1504–1514. http://dx.doi.org/10.1093/cercor/bhn163

Rathod, R., S. Havlicek, N. Frank, R. Blum, and M. Sendtner. 2012. Laminin induced local axonal translation of β-actin mRNA is impaired in SMN-deficient motoneurons. *Histochem. Cell Biol.* 138:737–748. http://dx.doi.org/10.1007/s00418-012-0989-1

Rehberg, M., A. Lepier, B. Solchenberger, P. Osten, and R. Blum. 2008. A new non-disruptive strategy to target calcium indicator dyes to the endoplasmic reticulum. *Cell Calcium.* 44:386–399. http://dx.doi.org/10.1016/j.ceca.2008.02.002

Rossoll, W., S. Jablonka, C. Andreassi, A.K. Kröning, K. Karle, U.R. Monani, and M. Sendtner. 2003. Smn, the spinal muscular atrophy-determining gene product, modulates axon growth and localization of beta-actin mRNA in growth cones of motoneurons. *J. Cell Biol.* 163:801–812. http://dx.doi.org/10.1083/jcb.200304128

Rubenstein, P.A. 1990. The functional importance of multiple actin isoforms. *BioEssays.* 12:309–315. http://dx.doi.org/10.1002/bies.950120702

Saal, L., M. Briese, S. Kneitz, M. Glinka, and M. Sendtner. 2014. Subcellular transcriptome alterations in a cell culture model of spinal muscular atrophy point to widespread defects in axonal growth and presynaptic differentiation. *RNA.* 20:1789–1802. http://dx.doi.org/10.1261/rna.047373.114

Schildmeyer, L.A., R. Braun, G. Taffet, M. Debiasi, A.E. Burns, A. Bradley, and R.J. Schwartz. 2000. Impaired vascular contractility and blood pressure homeostasis in the smooth muscle α-actin null mouse. *FASEB J.* 14:2213–2220. http://dx.doi.org/10.1096/fj.99-0927com

Schneider, C.A., W.S. Rasband, and K.W. Eliceiri. 2012. NIH Image to ImageJ: 25 years of image analysis. *Nat. Methods.* 9:671–675. http://dx.doi.org/10.1038/nmeth.2089

Schreiber, J., M.J. Végh, J. Dawitz, T. Kroon, M. Loos, D. Labonté, K.W. Li, P. Van Nierop, M.T. Van Diepen, C.I. De Zeeuw, et al. 2015. Ubiquitin ligase TRIM3 controls hippocampal plasticity and learning by regulating synaptic γ-actin levels. *J. Cell Biol.* 211:569–586. http://dx.doi.org/10.1083/jcb.201506048

Schwab, M.E. 2004. Nogo and axon regeneration. *Curr. Opin. Neurobiol.* 14:118–124. http://dx.doi.org/10.1016/j.conb.2004.01.004

See, K., P. Yadav, M. Giegerich, P.S. Cheong, M. Graf, H. Vyas, S.G. Lee, S. Mathavan, U. Fischer, M. Sendtner, and C. Winkler. 2014. SMN deficiency alters Nrxn2 expression and splicing in zebrafish and mouse models of spinal muscular atrophy. *Hum. Mol. Genet.* 23:1754–1770. http://dx.doi.org/10.1093/hmg/ddt567

Simon, C.M., S. Jablonka, R. Ruiz, L. Tabares, and M. Sendtner. 2010. Ciliary neurotrophic factor-induced sprouting preserves motor function in a mouse model of mild spinal muscular atrophy. *Hum. Mol. Genet.* 19:973–986. http://dx.doi.org/10.1093/hmg/ddp562

Sivadasan, R., D. Hornburg, C. Drepper, N. Frank, S. Jablonka, A. Hansel, X. Lojewski, J. Sterneckert, A. Hermann, P.J. Shaw, et al. 2016. C9ORF72

interaction with cofilin modulates actin dynamics in motor neurons. *Nat. Neurosci.* 19:1610–1618. http://dx.doi.org/10.1038/nn.4407

Sonnemann, K.J., D.P. Fitzsimons, J.R. Patel, Y. Liu, M.F. Schneider, R.L. Moss, and J.M. Ervasti. 2006. Cytoplasmic γ-actin is not required for skeletal muscle development but its absence leads to a progressive myopathy. *Dev. Cell.* 11:387–397. http://dx.doi.org/10.1016/j.devcel.2006.07.001

Spillane, M., A. Ketschek, S.L. Jones, F. Korobova, B. Marsick, L. Lanier, T. Svitkina, and G. Gallo. 2011. The actin nucleating Arp2/3 complex contributes to the formation of axonal filopodia and branches through the regulation of actin patch precursors to filopodia. *Dev. Neurobiol.* 71:747–758. http://dx.doi.org/10.1002/dneu.20907

Spillane, M., A. Ketschek, C.J. Donnelly, A. Pacheco, J.L. Twiss, and G. Gallo. 2012. Nerve growth factor-induced formation of axonal filopodia and collateral branches involves the intra-axonal synthesis of regulators of the actin-nucleating Arp2/3 complex. *J. Neurosci.* 32:17671–17689. http://dx.doi.org/10.1523/JNEUROSCI.1079-12.2012

Spillane, M., A. Ketschek, T.T. Merianda, J.L. Twiss, and G. Gallo. 2013. Mitochondria coordinate sites of axon branching through localized intra-axonal protein synthesis. *Cell Reports.* 5:1564–1575. http://dx.doi.org/10.1016/j.celrep.2013.11.022

Tam, S.L., and T. Gordon. 2003. Mechanisms controlling axonal sprouting at the neuromuscular junction. *J. Neurocytol.* 32:961–974. http://dx.doi.org/10.1023/B:NEUR.0000020635.41233.0f

Taneja, K.L., and R.H. Singer. 1990. Detection and localization of actin mRNA isoforms in chicken muscle cells by in situ hybridization using biotinated oligonucleotide probes. *J. Cell. Biochem.* 44:241–252. http://dx.doi.org/10.1002/jcb.240440406

Taylor, A.M., D.C. Dieterich, H.T. Ito, S.A. Kim, and E.M. Schuman. 2010. Microfluidic local perfusion chambers for the visualization and manipulation of synapses. *Neuron.* 66:57–68. http://dx.doi.org/10.1016/j.neuron.2010.03.022

Tondeleir, D., A. Lambrechts, M. Müller, V. Jonckheere, T. Doll, D. Vandamme, K. Bakkali, D. Waterschoot, M. Lemaistre, O. Debeir, et al. 2012. Cells lacking β-actin are genetically reprogrammed and maintain conditional migratory capacity. *Mol. Cell. Proteomics.* 11:255–271. http://dx.doi.org/10.1074/mcp.M111.015099

Van Baelen, H., R. Bouillon, and P. De Moor. 1980. Vitamin D-binding protein (Gc-globulin) binds actin. *J. Biol. Chem.* 255:2270–2272.

Vandekerckhove, J., and K. Weber. 1978. At least six different actins are expressed in a higher mammal: An analysis based on the amino acid sequence of the amino-terminal tryptic peptide. *J. Mol. Biol.* 126:783–802. http://dx.doi.org/10.1016/0022-2836(78)90020-7

Wallgren-Pettersson, C., K. Pelin, K.J. Nowak, F. Muntoni, N.B. Romero, H.H. Goebel, K.N. North, A.H. Beggs, and N.G. Laing. 2004. Genotype-phenotype correlations in nemaline myopathy caused by mutations in the genes for nebulin and skeletal muscle α-actin. *Neuromuscul. Disord.* 14:461–470. http://dx.doi.org/10.1016/j.nmd.2004.03.006

Wiese, S., F. Metzger, B. Holtmann, and M. Sendtner. 1999. The role of p75NTR in modulating neurotrophin survival effects in developing motoneurons. *Eur. J. Neurosci.* 11:1668–1676. http://dx.doi.org/10.1046/j.1460-9568.1999.00585.x

Wiese, S., T. Herrmann, C. Drepper, S. Jablonka, N. Funk, A. Klausmeyer, M.L. Rogers, R. Rush, and M. Sendtner. 2010. Isolation and enrichment of embryonic mouse motoneurons from the lumbar spinal cord of individual mouse embryos. *Nat. Protoc.* 5:31–38. http://dx.doi.org/10.1038/nprot.2009.193

Willis, D.E., E.A. van Niekerk, Y. Sasaki, M. Mesngon, T.T. Merianda, G.G. Williams, M. Kendall, D.S. Smith, G.J. Bassell, and J.L. Twiss. 2007. Extracellular stimuli specifically regulate localized levels of individual neuronal mRNAs. *J. Cell Biol.* 178:965–980. http://dx.doi.org/10.1083/jcb.200703209

Willis, D.E., M. Xu, C.J. Donnelly, C. Tep, M. Kendall, M. Erenstheyn, A.W. English, N.C. Schanen, C.B. Kirn-Safran, S.O. Yoon, et al. 2011. Axonal Localization of transgene mRNA in mature PNS and CNS neurons. *J. Neurosci.* 31:14481–14487. http://dx.doi.org/10.1523/JNEUROSCI.2950-11.2011

Z'Graggen, W.J., G.A. Metz, G.L. Kartje, M. Thallmair, and M.E. Schwab. 1998. Functional recovery and enhanced corticofugal plasticity after unilateral pyramidal tract lesion and blockade of myelin-associated neurite growth inhibitors in adult rats. *J. Neurosci.* 18:4744–4757.

Zhang, W., and D.L. Benson. 2001. Stages of synapse development defined by dependence on F-actin. *J. Neurosci.* 21:5169–5181.

Zhang, H.L., T. Eom, Y. Oleynikov, S.M. Shenoy, D.A. Liebelt, J.B. Dictenberg, R.H. Singer, and G.J. Bassell. 2001. Neurotrophin-induced transport of a beta-actin mRNP complex increases β-actin levels and stimulates growth cone motility. *Neuron.* 31:261–275. http://dx.doi.org/10.1016/S0896-6273(01)00357-9

Zheng, J.Q., T.K. Kelly, B. Chang, S. Ryazantsev, A.K. Rajasekaran, K.C. Martin, and J.L. Twiss. 2001. A functional role for intra-axonal protein synthesis during axonal regeneration from adult sensory neurons. *J. Neurosci.* 21:9291–9303.